Journal of Biomolecular Structure & Dynamics, ISSN 0739-1102
Volume 18, Issue Number 6, (2001)


# The First Example of a Hoogsteen Basepaired DNA Duplex in Dynamic Equilibrium with a Watson-Crick Basepaired Duplex – A Structural (NMR), Kinetic and Thermodynamic Study

http://www.adeninepress.com

**J. Isaksson,**
**E. Zamaratski,**
**T. V. Maltseva,**
**P. Agback,**
**A. Kumar, and**
**J. Chattopadhyaya***

Department of Bioorganic Chemistry, Box 581, Biomedical Centre, University of Uppsala, Sweden

***Abstract***

A single-point substitution of the O4' oxygen by a $CH_2$ group at the sugar residue of $\underline{A}^6$ (i.e. 2'-deoxyaristeromycin moiety) in a self-complementary DNA duplex, 5'-d($C^1G^2C^3G^4A^5A^6T^7T^8C^9G^{10}C^{11}G^{12}$)$_2$-3', has been shown to steer the *fully* Watson-Crick basepaired DNA duplex (1A), akin to the native counterpart, to a doubly $\underline{A}^6$:$T^7$ Hoogsteen basepaired (**1B**) B-type DNA duplex, resulting in a dynamic equilibrium of (**1A**)⇄(**1B**): $K_{eq} = k_1/k_{-1} = 0.56\pm0.08$. The dynamic conversion of the *fully* Watson-Crick basepaired (**1A**) to the partly Hoogsteen basepaired (**1B**) structure is marginally kinetically and thermodynamically disfavoured [$k_1$ (298K) = 3.9± 0.8 $sec^{-1}$; $\Delta H^{o\ddagger}$ = 164±14 kJ/mol; $-T\Delta S^{o\ddagger}$ (298K) = -92 kJ/mol giving a $\Delta G^{o\ddagger}_{298}$ of 72 kJ/mol. Ea (k1) = 167±14 kJ/mol] compared to the reverse conversion of the Hoogsteen (1B) to the Watson-Crick (1A) structure [k-1 (298K) = 7.0± 0.6 sec-1, $\Delta H^{o\ddagger}$ = 153±13 kJ/mol; $-T\Delta S^{o\ddagger}$ (298K) = -82 kJ/mol giving a $\Delta G^{o\ddagger}_{298}$ of 71 kJ/mol. Ea (k-1) = 155±13 kJ/mol]. A comparison of $\Delta G^{o\ddagger}_{298}$ of the forward (k1) and backward (k-1) conversions, (**1A**)⇄(**1B**), shows that there is ca 1 kJ/mol preference for the Watson-Crick (**1A**) over the double Hoogsteen basepaired (**1B**) DNA duplex, thus giving an equilibrium ratio of almost 2:1 in favour of the fully Watson-Crick basepaired duplex. The chemical environments of the two interconverting DNA duplexes are very different as evident from their widely separated sets of chemical shifts connected by temperature-dependent exchange peaks in the NOESY and ROESY spectra. The fully Watson-Crick basepaired structure (**1A**) is based on a total of 127 intra, 97 inter and 17 cross-strand distance constraints per strand, whereas the double $\underline{A}^6$:$T^7$ Hoogsteen basepaired (**1B**) structure is based on 114 intra, 92 inter and 15 cross-strand distance constraints, giving an average of 22 and 20 NOE distance constraints per residue and strand, respectively. In addition, 55 NMR-derived backbone dihedral constraints per strand were used for both structures. The main effect of the Hoogsteen basepairs in (**1B**) on the overall structure is a narrowing of the minor groove and a corresponding widening of the major groove. The Hoogsteen basepairing at the central $\underline{A}^6$:$T^7$ basepairs in (**1B**) has enforced a syn conformation on the glycosyl torsion of the 2'-deoxyaristeromycin moiety, $\underline{A}^6$, as a result of substitution of the endocyclic 4'-oxygen in the natural sugar with a methylene group in $\underline{A}^6$. A comparison of the Watson-Crick basepaired duplex (**1A**) to the Hoogsteen basepaired duplex (**1B**) shows that only a few changes, mainly in α, σ and γ torsions, in the sugar-phosphate backbone seem to be necessary to accommodate the Hoogsteen basepair.

Chemically modified oligonucleotides have played an important role in antisense therapy due to their cellular stability as well as effective cellular penetration compared to their natural DNA and RNA counterparts. The important features of any successful antisense oligonucleotide are (i) strong and specific binding to the target RNA strand, (ii) resistance to nucleolytic degradation, (iii) effective cellular penetration and (iv) rapid cleavage of antisense-RNA hybrid by cellular RNAse H. It has been found (1, 2) that when RNAse H is the target enzyme, it is essential that

Email:jyoti@bioorgchem.uu.se
Tel: +4618-4714577
Fax: +4618-554495

the antisense strand retains its B-DNA-like structure, while the RNA strand retains its original A-RNA like structure because of the substrate specificity of RNAse $H^1$. Although much is known (1) about the thermal stability of the binding of modified antisense DNA to natural DNA or RNA strands, few structural studies (3,4) in solution have been carried out on duplexes of chemically modified oligonucleotides in order to correlate structure, activity and stability at a molecular level.

Carbocyclic nucleoside analogues are interesting because of the following reasons: (i) Carbocyclic nucleosides are known (5) to be more resistant to glycosidic cleavage by cellular nucleases as well as by general acidic conditions. (ii) Oligos containing carbocyclic nucleotide moieties have thermodynamic stabilities very comparable to their natural counterparts (1,4). (iii) Most importantly, these carbocyclic nucleosides are devoid of intramolecular stereoelectronic gauche and anomeric effects (6) because of the absence of endocyclic O4'. Since these stereoelectronic forces (7) have been shown to be important in dictating a preferred conformation to the pentose sugar in natural nucleosides, we (6) and others (1b,8) have argued that incorporation of a carbocyclic nucleotide at a specific site in an oligo-DNA might be a way to induce flexibility in the local structure around it.

We herein report (9) our solution NMR studies of a Dickerson-Drew dodecamer, $^{5'}$-d($C^1G^2C^3G^4A^5A^6T^7T^8C^9G^{10}C^{11}G^{12}$)$_2$-$^{3'}$ (1), in which the pentose-sugar moiety of the 2'-deoxyadenosine residue $\underline{A}^6$ (Figure 1A) has been replaced by a carbocyclic analogue, 2'-deoxyaristeromycin, $\underline{A}^6$ (Figure 1B).

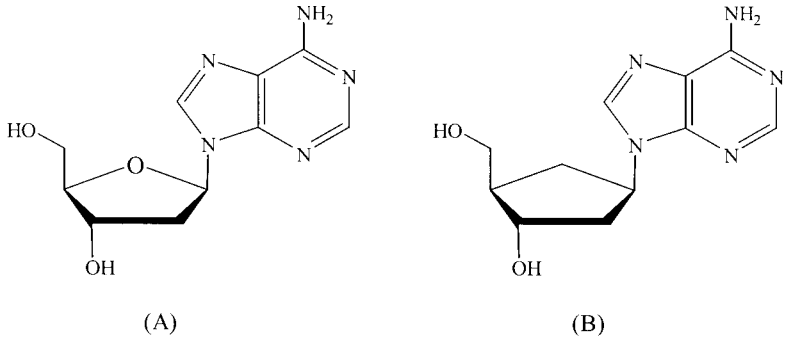


**Figure 1.** The structures of 2'-deoxyadenosine (A) and 2'-deoxyaristeromycin (B).

The results of the solution conformation studies on the 2'-deoxyaristeromycin modified dynamically interconverting duplexes, (**1A**)⇄(**1B**), were compared to the corresponding native duplex (**2**). In the (**1A**) form, the duplex adopts a normal B-type DNA conformation where all basepairs are of Watson-Crick type as in the native counterpart (*4,10*). In the (**1B**) form, the basepairs formed between $\underline{A}^6$ and $T^7$ at the center of the duplex are of Hoogsteen type (for a Hoogsteen basepaired triplex, see [*11*]), while the rest of the duplex has Watson-Crick baseparing, adopting a typical B-type conformation (*4,10*). The two dynamically interconverting duplexes have distinctly different chemical environments as evident by the different chemical shifts of their constituent protons. The two sets of proton chemical shifts allowed us to quantitatively assess their structures in detail, thereby enabling us, for the first time, to show how two Hoogsteen basepairs at the centre influence the overall structure of a otherwise fully Watson-Crick basepaired B-type DNA helix. In this work, we have also investigated the thermodynamics and the kinetics of the Watson-Crick (**1A**)⇄ Hoogsteen (**1B**) equilibrium and compared the thermal stabilities of the modified duplex (**1**) and the non-modified duplex (**2**).

### *Materials and Methods*

*(1)Synthesis*

The DNA dodecamer [d(CGCGAATTCGCG)]$_2$ with 2'-deoxyaristeromycin (6b) residue, $\underline{A}^6$, was synthesised by phosphoramidite chemistry using the standard solid phase synthesis protocol on Applied Biosystem equipment (392 DNA/RNA

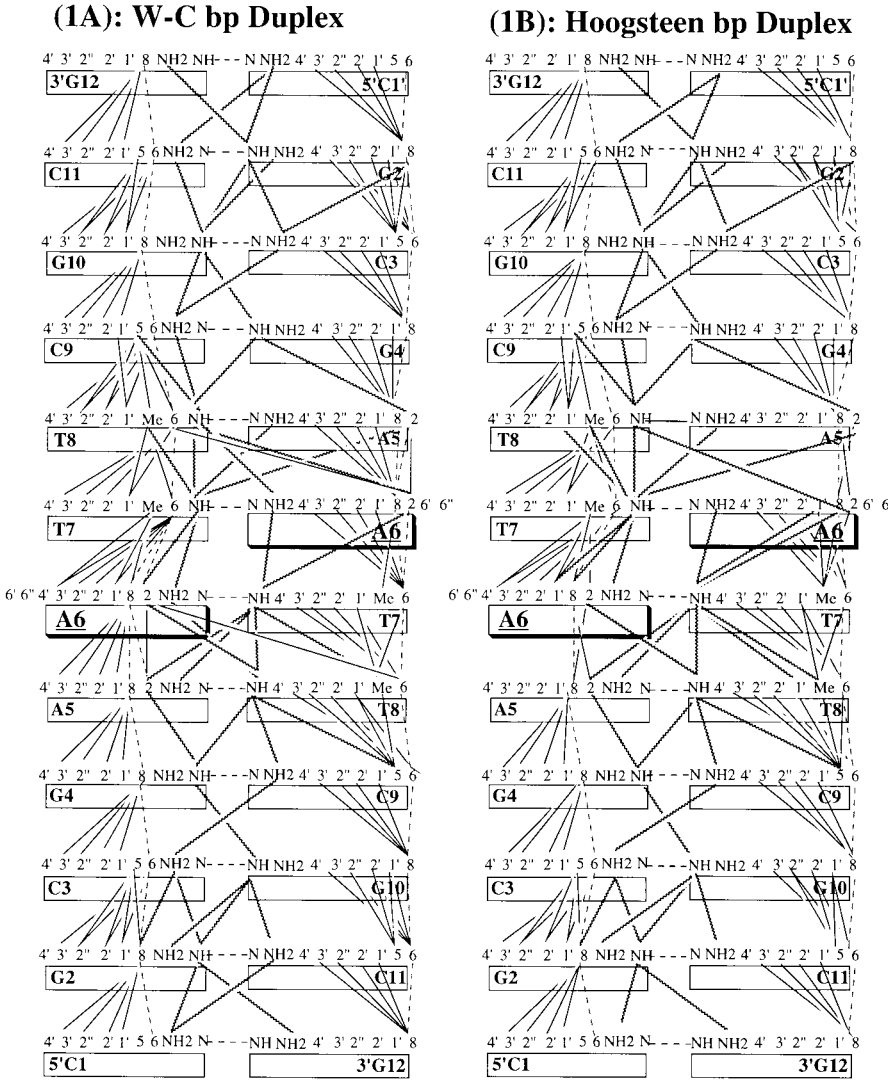


**Figure 2.** Schematic view of the interresidue NOEs from NOESY spectra used in the structure refinements as contraints. Note how both conformations show typical B-DNA type NOE connectivity pattern for the Watson-Crick basepaired residues ($C^1$-$A^5$ and $T^8$-$G^{12}$). The central Hoogsteen basepaired residues ($\underline{A}^6$-$T^7$) however are different and most significantly there is a break in H6/$8^n$-sugar $proton^{n-1}$ contacts between residue $A^5$ and $\underline{A}^6$, indicating a change in the base stacking in the centre of the duplex.

Synthesizer). The appropriate fractions were pooled to give 229 OD of duplex (1), which was found to be homoheneous by analytical HPLC (6c). This was lyophilised twice in D20 and dissolved in 0.6 ml D2O (99.96%) or in 9:1 $H_2O$:$D_2O$, v/v, containing 0.1 M NaCl, 0.01 M $PO_4^{3-}$, 0.001 M EDTA, pH 7.0 for NMR studies.

*(2)UV measurement*

UV melting profiles were obtained by scanning A260 absorbency versus time at a heating rate of 1ºC/min and a temperature gradient of 20-80ºC (60 min). The $T_m$s were calculated at each concentration from the maximums of the first derivatives of the melting curves. The Tm values used for the thermodynamic calculations were taken from the average of 5 melting experiments for the each concentration. All measurements were carried out in 0.2 M $Na_2HPO_4/NaH_2PO_4$, 1M NaCl buffer at pH 7.3. Before each melting experiment, denaturation and renaturation of the samples were carried out by heating solutions to 80ºC for 15 min followed by slow cooling to RT and storage in 20ºC overnight. Melting points at five different oligonucleotide concentrations (8, 12, 16, 20, and 24 μM total single strand concentration) were used for the calculations of ΔH, ΔS and ΔG. The resulting Tm values were fitted to a van't Hoff plot of $T_m^{-1}$ versus ln($C_T$), $C_T$ = total single strand concentration. The thermodynamics were calculated using equations 1 and 2:

$$1/Tm = (R/\Delta H^o)\ln C + \Delta S^o/\Delta H^o;\ R/\Delta H^o = \text{slope};\ \Delta S^o/\Delta H^o = \text{intercept} \quad (1)$$

$$\Delta G^o(298K) = \Delta H^o - T\Delta S^o; \quad (2)$$

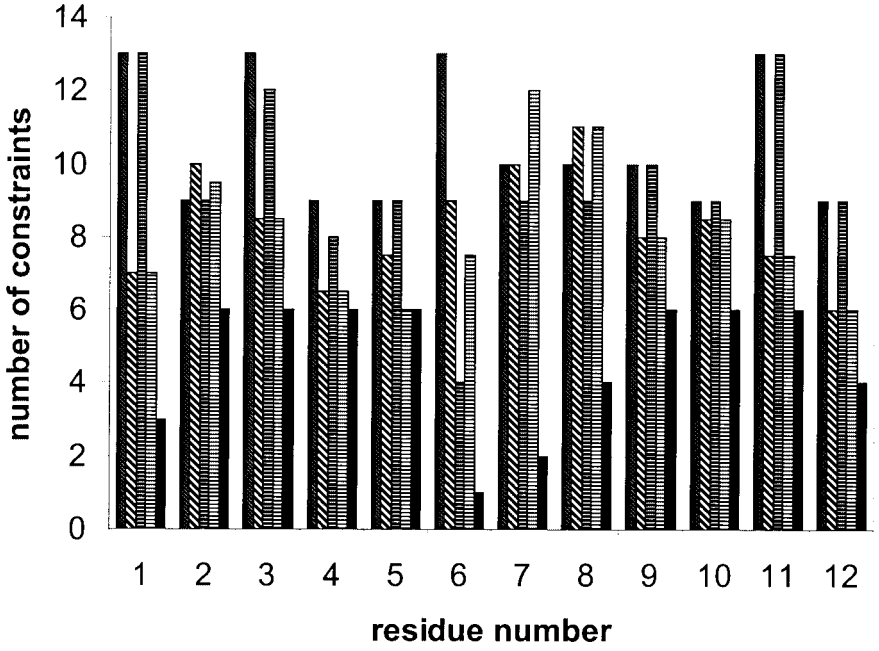


**Figure 3.** The distribution of the NMR derived NOE and dihedral constraints over the different residues for the Watson-Crick (**1A**) and Hoogsteen (**1B**) basepaired structures. The Watson-Crick structure (**1A**) showed the following NOEs: 127 intraresidue, 97 interresidue and 34 cross-strand, giving a total of 258 NOE constraints per strand. The Hoogsteen structure (**1B**) showed: 114 intraresidue, 92 interresidue and 30 cross-strand, giving a total of 236 NOE constraints per strand. This gives an average of 22 and 20 NOEs per residue and strand respectively. A total of 55 NMR-derived dihedral constraints per strand were also used to model both structures.

*(3) CD measurement*

CD experiments were performed using JASCO J41-A spectropolarimeter. CD spectra were recorded from 320 to 220 nm in 0.2 cm path length cuvettes. Spectra were obtained with a DNA duplex concentration of 8 μM in 1M NaCl, 200 mM phosphate (pH 7.3) at 20ºC. The temperature was kept constant by circulating water through the cuvette holder. A time constant of 16 s and a sensitivity of 20 x $10^{-2}$ mº/cm were used.

*(4) NMR spectroscopy*

All spectra were recorded on BRUKER DRX-500 and DRX-600 spectrometers operating at 500.03 MHz and 600.13 MHz for protons. Phase-sensitive NOESY experiments in $D_2O$ were run at 0, 20, 26, 32, 38, 50ºC using the following parameters: mixing times between 70 and 300 ms, 4K complex data points in the t2 dimension, 1K or 512 complex data points in the $t_1$ dimension, relaxation delay of 3 or 5s, sweep width of 10 ppm in both dimensions, 64 acquisitions per FID; a Lorenz apodization function for the $t_2$ dimension and a shifted sine-bell apodization function for the $t_1$ dimension. The data was zero-filled in $t_1$ to give 4K x 4K complex data points. All regions were base corrected separately. The residual water resonance was saturated with very low power during the relaxation delay. 2D NOESY in $H_2O$:$D_2O$ 9:1, v/v were run at 0 and 20ºC with mixing times of 70, 150 and 300 ms. The water signal was suppressed by the WATERGATE pulse sequence. To discriminate exchangeable crosspeaks from those arisen from dipole-dipole relaxation, a set of phase-sensitive NOESY and ROESY experiments have been performed. For NOESY experiments the water suppression was achieved by the use of two short spinlock pulses, $SL_{\psi 4}$ and $SL_{\psi 5}$ (*12*) using the following parameters: $SL_{\psi 4}$ and $SL_{\psi 5}$ are equal to 0.5μs and 3μs respectively, the delay between spinlock pulses is equal to 45 or 150μs, the carrier was set at the water frequency. For ROESY experiments, the water suppression was achieved with one short spinlock pulse, $SL_{\psi 3}$. The used sequence, during the mixing time, of n($\pi$/6) pulses with length 2.5μs separated by delay, Δ(34.5μs), corresponds to 6.25 kHz rf field power for pulses. This provides a similar effect as spinlock, $SL_{\psi 4}$, of the NOESY experiment.

Two-dimensional datasets for DQF-COSY spectra were collected in phase-sensitive mode with time-proportional phase incrementation, with and without phosphorus decoupling at 20 and 50ºC. Typically, 4k data points were collected for each

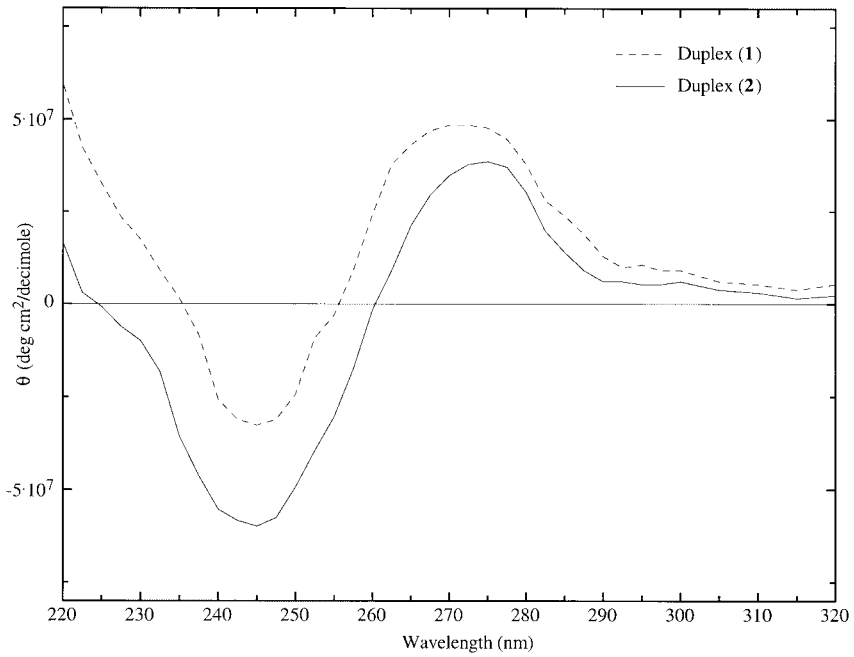


**Figure 4.** The CD spectra of the modified dodecamer (1, dashed line) compared to the natural counterpart (2, solid line): 8μM oligo in 1M NaCl, 200 mM phosphate (pH 7.3) at 20 ºC.

1k of $t_1$ values in the DQF-COSY experiments. The 4k x 2k data points were resolution-enhanced by a shifted square sine-bell window function in both the $t_1$ and $t_2$ dimensions, then Fourier transformed and phase adjusted. A relaxation delay of 3 s was used. Data was collected on non-spinning samples to avoid $t_1$ noise.

The inverse $^1H,^{31}P$-correlation (*13*) spectra were measured with the delay, τ, in the INEPT step adjusted to give $J_{HP}$ of 12 Hz, 256 scans and 256 experiments, all obtained at 20ºC.

See our website:http://bioorgchem.boc.uu.se for Figures in colour.

*(5) Structure refinement*

All structures were calculated by simulated annealing (SA) and refine protocols using X-PLOR 3.1 (*14*). The DNA force field parameters were modified as suggested by Varani (*15*). First, the SA-protocol of Omichinski et al (*16*) was applied with some modifications: The protocol starts with an initial phase comprising 10 ps of dynamics (5000 steps of 2 fs each) at 2000K with the following force constants: NOE: 2 kcal $mol^{-1}Å^{-2}$, dihedral: 10 kcal $mol^{-1}rad^{-2}$, bonds: 1000 kcal $mol^{-1}Å^{-2}$, angles: 200 kcal $mol^{-1}rad^{-2}$, impropers: 50 kcal $mol^{-1}rad^{-2}$, van der Waal: 1 kcal $mol^{-1}Å^{-4}$ (scale factor 1.2) and non-crystallographic symmetry (NCS): 5 kcal $mol^{-1}Å^{-2}$. This phase generates softly constrained structures with a random seed (RMSD between 3-7 ). In the next phase the system is cooled from 2000 to 100K over 76 cycles each of 0.316 ps (reducing the temperature by 25 K for each cycle). The NMR-derived dihedrals, 200 kcal mol-1rad-2, bond: 1000 kcal $mol^{-1}Å^{-2}$ and NCS: 5 kcal $mol^{-1}Å^{-2}$, are kept constant during this phase while the following are increased by the term (<initial>-<final>)/76 for each cycle: NOE: 2-30 kcal $mol^{-1}Å^{-2}$, angles: 200-500 kcal $mol^{-1}rad^{-2}$ and van der Waal: 0.004-4 kcal $mol^{-1}Å^{-4}$ (the radius scale factor for van der Waal is decreased from 0.9 to 0.8 during this phase). Finally, there are 500 steps of Powell minimisation.

Then the standard refine protocol (refine.inp) was applied two times in succession with cooling from 1000K to 100K and 500K to 100K respectively. The NCS was added with a force constants of 10 kcal $mol^{-1}Å^{-2}$ during this protocol. The number of cooling steps was increased to 10000 and the number of Powell minimisation steps to 1000 in this protocol. The force constants are 50 kcal $mol^{-1}Å^{-2}$ for NOE, 200 kcal $mol^{-1}rad^{-2}$ for dihedrals, 1000 kcal $mol^{-1}Å^{-2}$ for bonds, 500 kcal $mol^{-1}rad^{-2}$ for

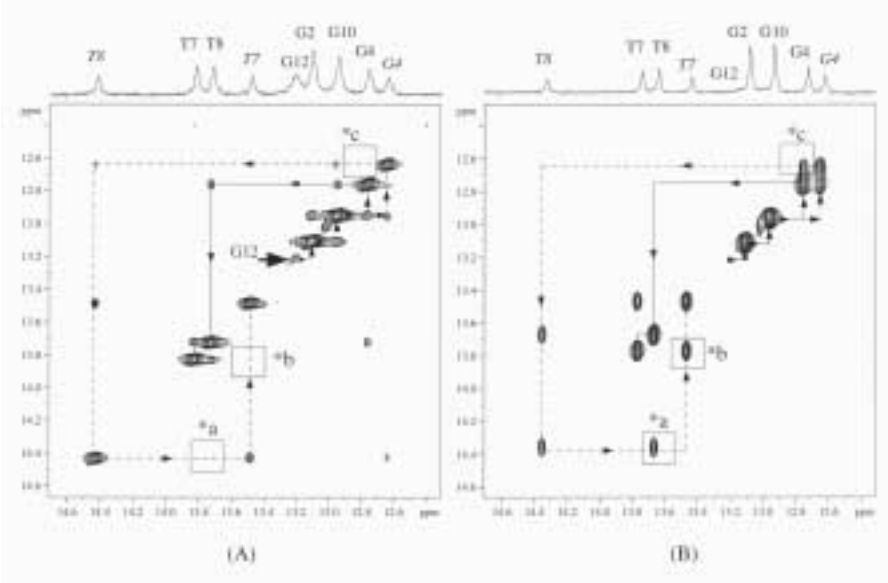


**Figure 5.** Two sets of sequential imino-imino NOEs can be traced at 0C (panel A) and 20C (panel B)for [5–d($C^1G^2C^3G^4A^5A^6T^7T^8C^9G^{10}C^{11}G^{12}$)-3']$^2$. The terminal residues ($G^2$, $G^{10}$, $G^{12}$) of the Watson-Crick basepaired set (**1A**, solid lines, plain font) and the Hoogsteen basepaired set (**1B**, dashed lines, italic font) have isochronous chemical shifts while the central ones (residue $G^4$, $T^7$, $T^8$) show significant differences in chemical shifts. Note that at 20ºC the central imino protons of the two traces show exchange crosspeaks (boxes a, b and c). See our website:http://bioorgchem.boc.uu.se for Figures in colour.

angles, 500 kcal mol$^{-1}$rad$^{-2}$ for impropers, 0.1-4 kcal mol$^{-1}$Å$^{-4}$ for van der Waal and 10 kcal mol$^{-1}$Å$^{-2}$ for NCS.

The starting structure for the calculations was two stretched out DNA-strands of A- and B-type aligned antiparallel to each other. For each of the possible basepairing alternatives (Watson-Crick and Hoogsteen) we calculated 50 structures from each DNA type, using either Watson-Crick or Hoogsteen base-pairing for the two $\underline{A}^6$-$T^7$ basepairs. After the SA-protocol and the two refinement protocols we accepted the structures that showed no NOE violations greater than 0.5 Å, no dihedral violations greater than 5º, RMSD deviation from ideal bond lengths < 0.01Å, RMSD deviation from ideal bond angle < 1º and energies no more than 15 kcal higher than the lowest energy structure as final structures. Due to the similarity between the constraints, we did a test calculation in which the Watson-Crick NOEs were combined with the Hoogsteen hydrogen bonding and vice versa. No structures converged during these calculations.

The final structures were compared to the NOE intensities using MARDIGRAS (*17*) in order to obtain an R-factor analysis.

The helical parameters were calculated, using the program by Babcock et al (*18*).

*(6) Coalescence simulation*

The simulation of the coalescence was made using equation 3 (19), describing the lineshape [g(n)].

where,

$$g(v)=\frac{(1+\tau\pi\Delta)P+QR}{4\pi^2P^2+R^2} \qquad (3)$$

$$P=(0.25\Delta^2-v^2+0.25\delta v^2)\tau+\Delta/_{4\pi}$$
$$Q=[-v-0.5(P_A-P_B)\delta v]\tau$$
$$R=0.5(P_A-P_B)\delta v-v(1+2\pi\tau\Delta)$$
$$\tau=\frac{\tau_A\tau_B}{\tau_{A+}\tau_B}$$

$\tau_A$, $\tau_B$ are the average life times of the nuclei in the Watson-Crick and Hoogsteen structure respectively.

$\rho A$, $\rho B$ are the molar fractions of the Watson-Crick and Hoogsteen structure.
$\delta\nu = \nu_A - \nu_B$ is the difference between the resonance frequencies of the nuclei of the Watson-Crick and Hoogsteen structure.

$\Delta$ is the width at half-height of the signal in the absence of exchange.

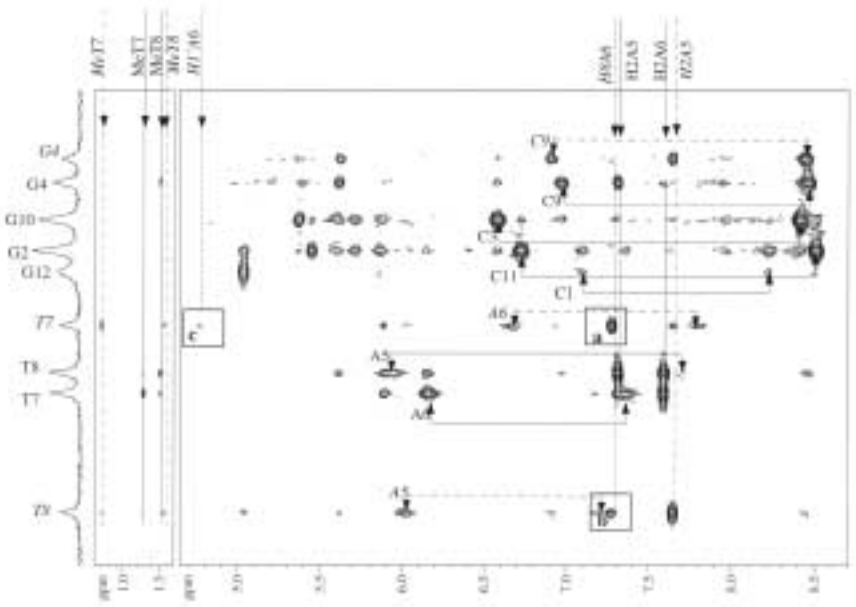

**Figure 6.** NOESY spectra in $H_2O$ at 0ºC showing imino-MeT/amino/H2 crosspeaks. Note the H8A$^6$-H3T$^7$ and T$^8$ (boxes: a and b) and H1'A6-H3T7 (box c) typical for Hoogsteen basepairing (solid lines, plain font: Watson-Crick [**1A**], dashed lines, *italic* font: Hoogsteen duplex [**1B**]). See our website: http://bioorgchem.boc.uu.se/ for Figures in colour.

n is the variable frequency.

*(7) Exchange kinetics*

A set of NOESY and ROESY spectra (T = 287, 290, 293, 298, 300, 303, 308 K; $t_m$ = 20, 50, 80, 120, 200, 400 ms) were used to calculate the interconversion exchange rates of structure (1A) and (1B). Rate constants of the exchange process, $k_1$ and $k_{-1}$, were calculated from the initial slope of crosspeak volume build-up using the program AURELIA V2.1.3 (20) for volume calculations. The energy of activation, $E_a$, of the process was obtained using equations 4, 5 and 6, and from that, the thermodynamics:

$$k_1 = A\exp\left(\frac{-Ea}{RT}\right) \quad (4)$$

$$E_a = \Delta H^{o\ddagger} + RT \quad (5)$$

$$k_1 = e^2\left(\frac{kT}{h}\right)\exp\left(\frac{\Delta S^{o\ddagger}}{R}\right)\exp\left(\frac{-E_a}{RT}\right) \quad (6)$$

The intensities of pure exchange crosspeaks in NOESY as a function of mixing time, $\tau_m$, are described by equation 7. A more detailed discussion about exchange theory can be found in reference (*21*).

$$a_{A1A2} = \frac{m^0_{A_1}}{2} k_1 \left\{ \frac{1}{A}\left(e^{-\lambda_1\tau_m} - e^{-\lambda_3\tau_m}\right) + \frac{1}{D}\left(e^{-\lambda_2\tau_m} - e^{-\lambda_4\tau_m}\right) \right\} \quad (7)$$

$$A = \sqrt{4k_1k_{-1} + (k_1 - k_{-1} + \rho_1 - \rho_2 + \sigma_1 - \sigma_2)^2}$$

$$D = \sqrt{4k_1k_{-1} + (k_1 - k_{-1} + \rho_1 - \rho_2 - \sigma_1 + \sigma_2)^2}$$

$m_{A1}{}^0$ is the initial magnetisation at $\tau_m$ = 0, $k_1$ and $k_{-1}$ are the rate constants and $\lambda$1-4 are the eigenvalues of the dynamic matrix describing longitudinal relaxation and chemical exchange.

The time derivative of equation 7 shows that the slope at $\tau_m$=0 equals $m_{A1}{}^0k_1$. Assuming exponential relaxation, the initial magnetisation of each proton is obtained by extrapolating the decaying volume of the diagonal peak on a logarithmic scale, thus giving $k_1$. The relations described by equations 8 and 9 are used to calculate $k_{-1}$.

$$M_{0A} = m_{0A_1} + m_{0A_2} \quad (8)$$

$$K_{eq} = k_1 / k_{-1} = m_{0A_1} / m_{0A_2} \quad (9)$$

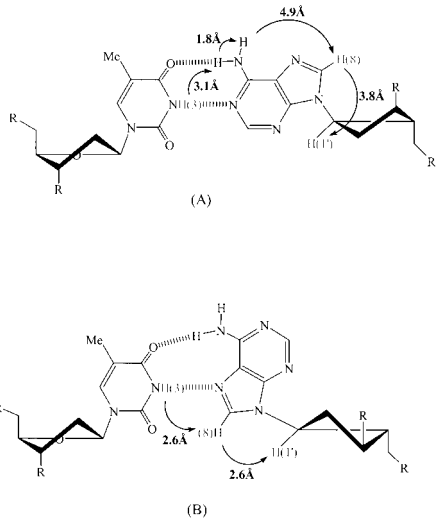


**Figure 7.** Schematic view of two A-T basepairs showing various key distances amongst imino-amino-aromatic-sugarH1' in a Watson-Crick (A) visá-vis a Hoogsteen (B) (*9a,10*) basepair. For the Hoogsteen basepaired structure (B), magnetisation transfer from H3T$^7$ to H1'$\underline{A}^6$ is possible, through both direct dipolar interaction (5.1 Å) and through spin diffusion through H$^8\underline{A}^6$. The syn conformation across the glycosidic bond of the adenosine nucleotide brings the H3T$^7$ and H$^8\underline{A}^6$ (2.6 Å) as well as H8A6 and H1'$\underline{A}^6$ (2.6Å) into close proximity of each other. The same crosspeak for the Watson-Crick basepaired structure (A), with both aglycons in *anti* conformations, is however expected to be much weaker (or not observable) under normal conditions because the magnetisation would have to be transferred 6.8Å through space or by spin diffusion through 4 steps covering a total distance of 13.6Å (3.1 + 1.8 + 4.9 + 3.8Å).

## Results and Discussions

*(1) CD data*

A typical distinction between A- and B-type DNA is possible in CD spectra on the basis of the ratio between positive and negative ellipticity, the shift of crossover point as well as on the drift of the absorption maximum for the positive and negative peak. The structural transitions and thermodynamic properties obtained by UV are based on hyperchromism. It has been found that the CD is relatively a more sensitive tool to understand structural transitions, for example the transition between hairpin and random coil in DNA (*22a*), than UV. We have measured CD spectra of the modified duplex, [(**1A**)⇄(**1B**)], and compared to the natural counterpart (**2**) (Figure 4). As expected, the CD spectra of the native Dickerson-Drew dodecamer duplex are almost identical to those of large native DNAs (*4,22*). They show negative and positive CD bands of moderate magnitudes at 244 and 275 nm respectively (ratio of positive to negative lobes is 0.64) and crossover points at 224 and 260 nm, which are characteristic features (*22*) for B-DNA conformation (*4,10*). Substitution of the central 2'-deoxyadenosine nucleotides by the carbocyclic counterpart, 2'-deoxyaristeromycin, in Dickerson-Drew 12mer (**1**) shows some marked changes in the CD spectrum: The positive maximum $\lambda_{max}$ and the second crossover point are shifted to the shorter wavelengths; 270 nm and 253 nm respectively. Although $\lambda_{min}$ for the modified duplex (**1**) did not shift, the depth of the $\lambda_{min}$ at 245 nm was significantly reduced bringing the ratio between positive to negative magnitudes to 1.43, which is a distinctive A-type DNA feature (*22b*). However, our NMR data shows that this is not the case (see below). It is also noteworthy that the first crossover is shifted from 224 nm to 236 nm which is characteristic intermediate state (*22c*) for B→A transition. As the presence of a single-strand hairpin loop does not influence the appearance of CD spectra of a B-DNA duplex (*22d*), the observed changes in CD parameters cannot be explained by any loop formation but rather a change in the typical B-DNA helix structure. The quantitative deviation of the 2'-deoxyaristeromycin modified 12mer from the native B-DNA 12mer (*4*) is reflected in its RMS value of 2.15.

*(2) Assignment of the exchangeable protons*

For the native self-complementary dodecamer (**2**), we observe six imino proton resonances at low temperature (H$^1$ of G$^2$, G$^4$, G$^{10}$ and G$^{12}$ and H3 of T$^7$ and T$^8$). There are however nine imino proton peaks in the 1D spectra of duplex (**1**) at 0ºC (Figure 5A). Three of those resonances are connected to three other imino protons through chemical exchange crosspeaks in ROESY spectra at 20ºC (Figure 5B). The resonances showing exchange crosspeaks were, after assignment, found to be the imino

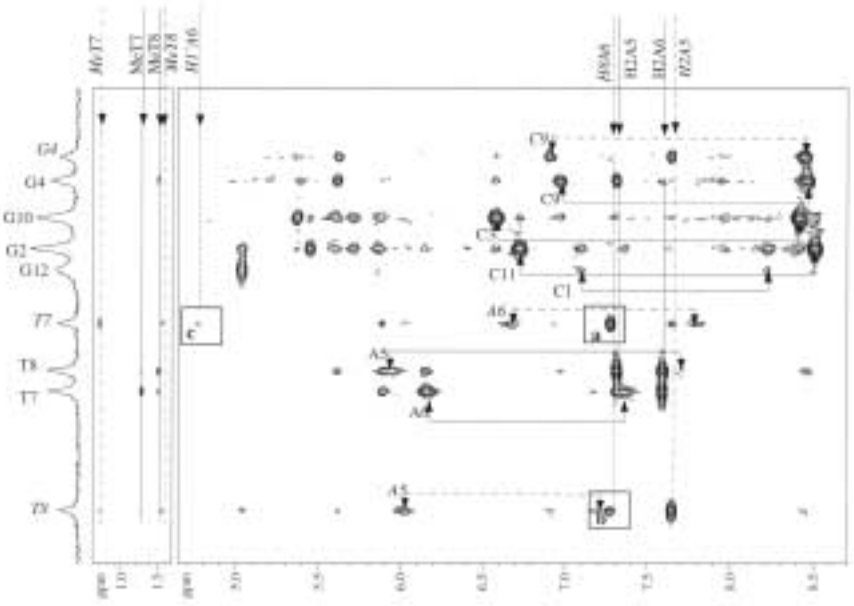

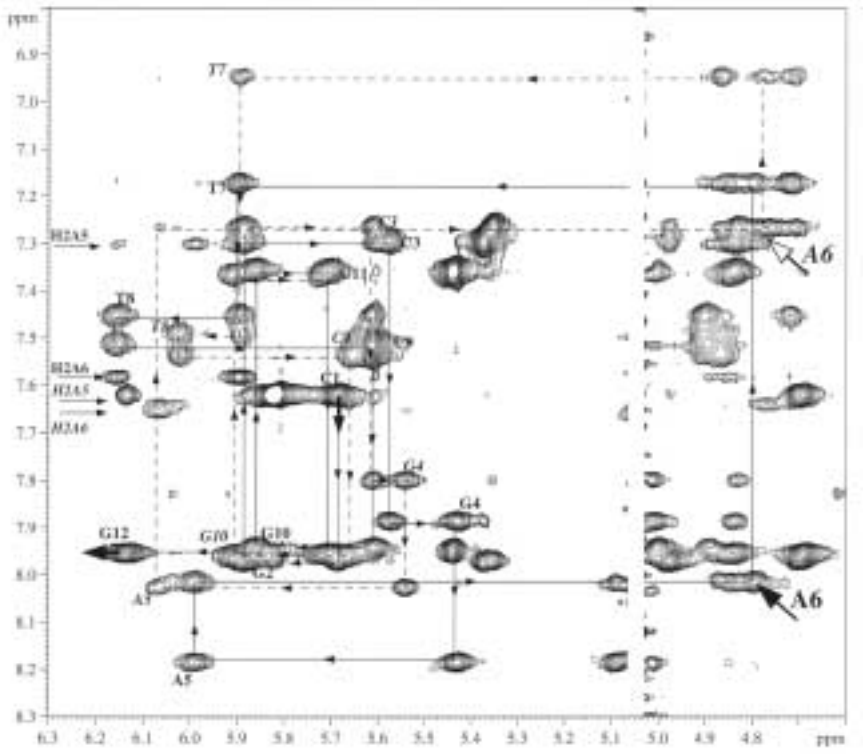


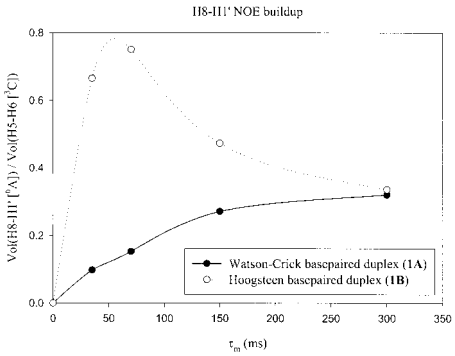


**Figure 8.** (A) NOESY spectra of the aroamtic-H1' region at 0C. Note the strong H8A$^6$-H1'A$^6$ NOE (marked with arrow) indicating a syn conformation (solid lines, plain font: Watson-Crick [1A], dashed lines, italic font: Hoogsteen duplex [**1B**]). See our website: http://bioorgchem.boc.uu.se/ for Figures in colour. (B) The quicker NOE buildup for the H8A6-H1'A6 NOE belonging to the Hoogsteen basepaired duplex (**1B**) indicates a syn conformation (solid lines, plain font: Watson-Crick [**1A**], dashed lines, *italic* font: Hoogsteen duplex [**1B**]). The H8A$^6$-H1'A$^6$ NOE volume of each duplex has been normalised against its H5-H6 crosspeak of residue C3 respectively.

protons of G$^4$, T$^7$ and T$^8$. The NOEs between the imino protons could be traced in two different ways (Figure 5A). Both start at the G$^{12}$ which is connected to G$^2$ which in turn is connected to G$^{10}$, there the connectivity splits into two, each connecting to a G$^4$ followed by T$^7$ and T$^8$. One of the assignment traces, assigned to

**Table I.**
Proton[a] and phosphorus[b] chemical shifts (ppm) for the two conformations of the modified duplex (**1A** and **1B**) compared to the native dodecamer (**2**)[c].

| Residue | Duplex | H6/H8 | H5/Me/H2 | H1' | H2' | H2'' | H3' | H4' | Amino | Imino |
|---|---|---|---|---|---|---|---|---|---|---|
| C$^1$ | (1A) | 7.62 | 5.82 | 5.68 | 1.96 | 2.41 | 4.69 | 4.36 | 8.22/7.10 | - |
| | (1B) | † | † | † | † | † | † | † | † | - |
| | (2) | 7.66 | 5.90 | 5.73 | 2.01 | 2.43 | 4.72 | 4.08 | | - |
| G$^2$ | (1A) | 7.96 | - | 5.88 | 2.65 | 2.72 | 4.98 | 4.36 | 5.85/5.70 | 13.11 |
| | (1B) | † | - | † | † | † | † | † | † | † |
| | (2) | 7.98 | - | 5.90 | 2.66 | 2.72 | 4.98 | 4.36 | | 13.13 |
| C$^3$ | (1A) | 7.29 | 5.37 | 5.57 | 1.90 | 2.30 | 4.84 | 4.15 | 8.41/6.58 | - |
| | (1B) | 7.26 | 5.35 | 5.61 | 1.87 | 2.29 | 4.83 | 4.16 | 8.41/6.58 | - |
| | (2) | 7.31 | 5.38 | 5.52 | 1.90 | 2.28 | 4.83 | 4.15 | | - |
| G$^4$ | (1A) | 7.88 | - | 5.43 | 2.67 | 2.74 | 5.01 | 4.33 | ‡ | 12.76 |
| | (1B) | 7.80 | - | 5.54 | 2.63 | 2.73 | 5.01 | 4.35 | ‡ | 12.64 |
| | (2) | 7.90 | - | 5.47 | 2.70 | 2.79 | 5.01 | 4.35 | | 12.73 |
| A$^5$ | (1A) | 8.12 | 7.30 | 5.99 | 2.76 | 2.85 | 5.09 | 4.47 | ‡/5.89 | - |
| | (1B) | 8.02 | 7.63 | 6.07 | 2.70 | 2.97 | 5.05 | 4.47 | 7.21/6.01 | - |
| | (2) | 8.15 | 7.19 | 6.02 | 2.72 | 2.98 | 5.08 | 4.50 | | - |
| A$^6$ (WC) | (1A) | 8.01 | 7.58 | 4.80 | 2.45 | 2.59 | 4.84 | 1.56 | 7.38/6.16 | - |
| A$^6$ (H) | (1B) | 6.95 | 7.65 | 4.77 | 2.23 | 2.52 | 4.71 | ‡ | 7.78/6.68 | - |
| A$^6$ | (2) | 8.17 | 7.63 | 6.19 | 2.58 | 2.97 | 5.02 | 4.49 | | - |
| T$^7$ (WC) | (1A) | 7.17 | 1.28 | 5.89 | 2.04 | 2.58 | 4.72 | 4.23 | - | 13.82 |
| T$^7$ (H) | (1B) | 6.95 | 0.70 | 5.89 | 1.79 | 2.49 | 4.86 | ‡ | - | 13.48 |
| T$^7$ | (2) | 7.18 | 1.26 | 5.95 | 2.02 | 2.61 | 4.86 | 4.24 | - | 13.83 |
| T$^8$ | (1A) | 7.45 | 1.51 | 6.15 | 2.15 | 2.57 | 4.90 | 4.23 | - | 13.72 |
| | (1B) | 7.48 | 1.56 | 6.02 | 2.27 | 2.51 | 4.90 | 4.20 | - | 14.43 |
| | (2) | 7.40 | 1.53 | 6.13 | 2.19 | 2.60 | 4.92 | 4.23 | - | 13.95 |
| C$^9$ | (1A) | 7.51 | 5.61 | 5.61 | 2.12 | 2.42 | 4.89 | 4.16 | 8.46/6.97 | - |
| | (1B) | 7.53 | 5.61 | 5.66 | 2.12 | 2.42 | 4.86 | 4.18 | 8.44/6.91 | - |
| | (2) | 7.49 | 5.60 | 5.70 | 2.08 | 2.45 | 4.90 | 4.18 | | - |
| G$^{10}$ | (1A) | 7.94 | - | 5.86 | 2.64 | 2.72 | 5.00 | 4.38 | ‡ | 12.94 |
| | (1B) | 7.95 | - | 5.91 | 2.64 | 2.72 | 5.00 | 4.40 | ‡ | 12.94 |
| | (2) | 7.95 | - | 5.85 | 2.67 | 2.70 | 5.01 | 4.39 | | 12.94 |
| C$^{11}$ | (1A) | 7.36 | 5.44 | 5.71 | 1.94 | 2.33 | 4.84 | 4.16 | 8.50/6.72 | - |
| | (1B) | † | † | † | † | † | † | † | † | - |
| | (2) | 7.38 | 5.45 | 5.72 | 1.94 | 2.35 | 4.84 | 4.18 | | - |
| G$^{12}$ | (1A) | 7.95 | - | 6.13 | 2.65 | 2.40 | 4.69 | 4.19 | 5.85/5.60 | 13.21 |
| | (1B) | † | - | † | † | † | † | † | † | † |
| | (2) | 7.98 | - | 6.17 | 2.65 | 2.36 | 4.70 | 4.20 | | 13.25 |

[a] Proton chemical shifts were measured at 0°C using DSS as reference (0.015 ppm).
[b] Phosphorus chemical shifts were measured at 20°C using trimethyl phosphate as external reference (0 ppm).
[c] The shaded area shows the residues with non-isochronous chemical shifts. The central residues (A$^6$ and T$^7$) that form Hoogsteen basepairs are shown between solid lines.
† The chemical shifts of both the Watson-Crick and Hoogsteen basepaired structures were isochronous.
‡ The corresponding crosspeak could not be assigned and/or there was too much overlap.

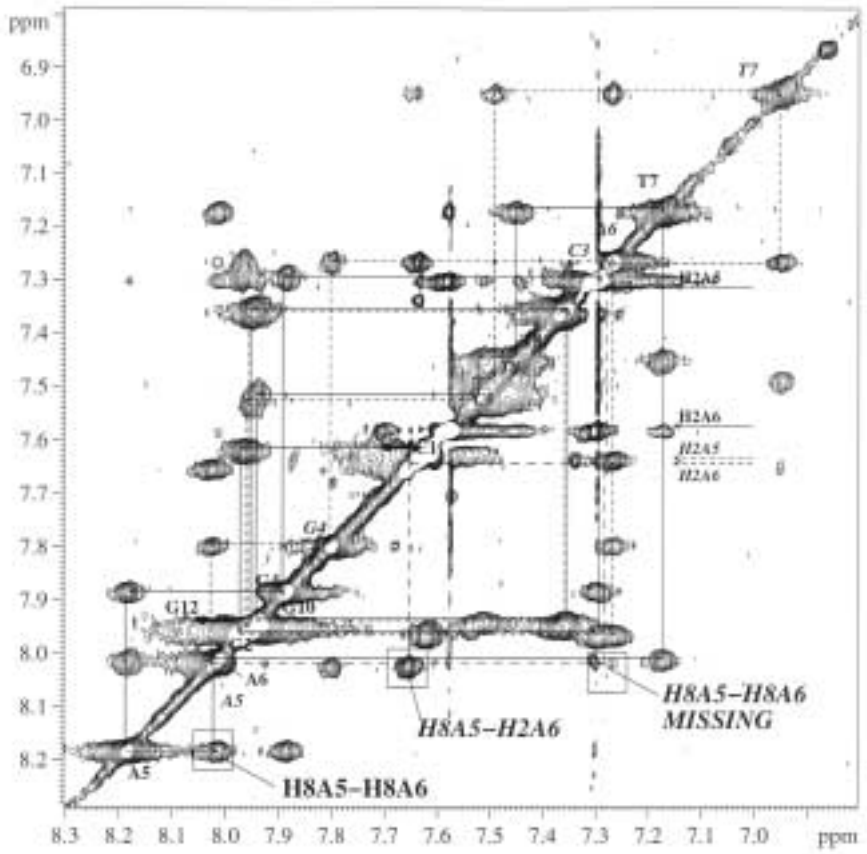


**Figure 9.** NOESY spectra recorded at 0ºC showing two sets of aromatic-aromatic NOEs. The Watson-Crick basepaired duplex (**1A**, solid lines, plain font) shows standard H8/H6 to H8/H6 interactions whereas in the Hoogsteen basepaired duplex (**1B**, dashed lines, *italic* font) there is an interruption between H8A$^5$ and H8$\underline{A}^6$. Instead there is a crosspeak between H8A$^5$ to H2$\underline{A}^6$ showing that there is most likely a flip of the glycosyl torsion, thus bringing them into a close proximity. See our website: http://bioorgchem.boc.uu.se/ for Figures in colour.

duplex (**1A**) [plain font for all assignments for (**1A**) in Figures 5, 6, 8 and 9], has similar chemical shifts to those of the native counterpart (2). The other trace, assigned to duplex (**1B**) [*italic* font for all assignments for (**1B**) in Figures 5, 6, 8 and 9] shows unusual chemical shifts (Table 1). The H3 imino protons of the central T$^7$ and T$^8$ residues belonging to duplex (**1B**) are shifted upfield by 0.33 ppm and downfield by 0.70 ppm respectively, indicating a change of the conformation at the centre of the DNA-duplex. All imino protons could be assigned to resonances between 12.5 and 14.5 ppm at 0ºC, and this enabled us to rule out the possibility of a hairpin structure at low temperatures, since the non-hydrogen bonded imino protons in the loop region of a hairpin structure are expected to have chemical shifts between 10.0 and 11.5 ppm (*23*). The set of unusual chemical shifts belonging to duplex (**1B**) is distinguished by NOESY crosspeaks between H3T$^7$ and H8A$^6$, H3T$^7$ and H1'$\underline{A}^6$ and between H3T$^8$ and H8$\underline{A}^6$ (Figure 6). These are NOEs associated with Hoogsteen basepairing (Figure 7) (11).

*(3) Assignment of the non-exchangeable protons*

As in the case of the imino protons, some residues have non-exchangeable resonances in duplicates. Those residues are: C$^3$, G$^4$, A$^5$, $\underline{A}^6$, T$^7$, T$^8$, C$^9$ and G$^{10}$, i.e. all except the terminal residues 1:12 and 2:11. In NOESY spectra below 50ºC, it is possible to trace assignments in two unique pathways from G$^2$ to C$^{11}$, each corresponding to a separate set of resonances (C$^1$ to G$^2$ and C$^{11}$ to G$^{12}$ are the same in both traces) (Figure 8). In both sets, the typical assignment pattern for DNA (*24*) can be followed, i.e. 5'-aromatic(n) →H1'/2'/2''/3'(n)→aromatic(n+1)-3'. In one of the assigned sets, the chemical shifts correspond very closely to the values of the published B-DNA type structure (*4,25*) of the native 12mer counterpart. However, several protons in the other set have unusual chemical shifts indicating deviation from typical B-DNA structure (Table 1). The imino protons with unusual shifts and NOEs also belong to this set. The H$^8$ of $\underline{A}^6$ is, for example, shifted upfield by 0.75 ppm compared to the other set at 0ºC. The H$^8$ of G$^4$, H$^8$ of A$^5$, H$^6$ of T$^7$ and MeT$^7$ are also shifted upfield by 0.09, 0.16, 0.23 and 0.58 ppm respectively at 0 ºC. The sugar protons of these residues are not shifted to any great extent (all less than 0.05

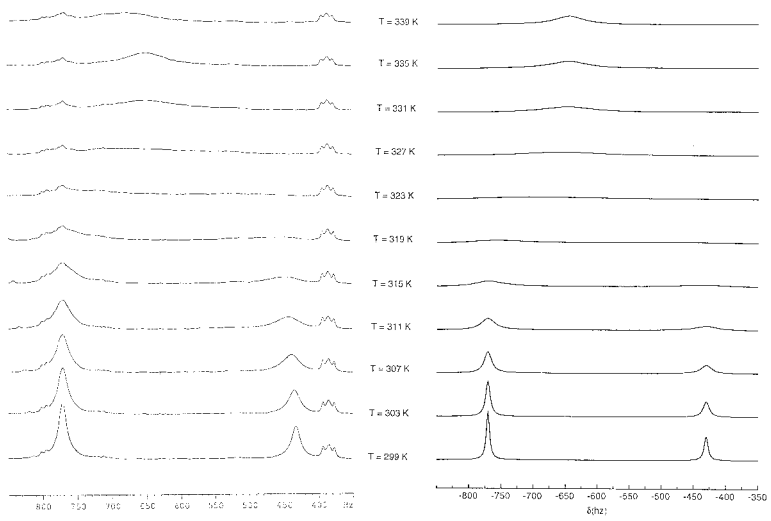


Figure 10A,B

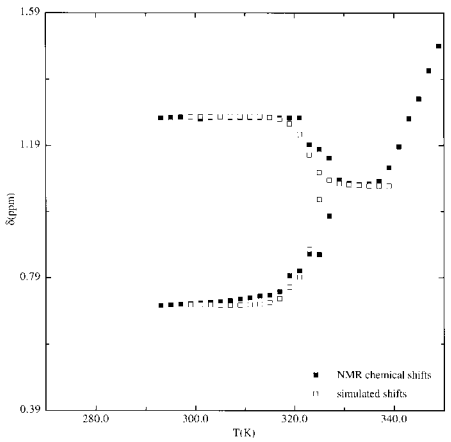


**Figure 10.** (A) Temperature-dependent 1D spectra of the coalescence process of two MeT$^7$ resonances (coming from the two duplex conformations) into one NMR time average signal. The resonance at 400 Hz belongs to an impurity that shows no temperature-dependent drift. (B) Lineshape simulation (18) of the coalescence process of the same two resonances of MeT$^7$ using the calculated rate constants, $k_1$ and $k_{-1}$ (extrapolated at temperatures above 25ºC), from the exchange studies, showing that the appearances of the experimental (A) and the simulated (B) spectra are virtually identical. (C) Comparison of the chemical shifts derived from the coalescence simulation (10B) and those of the experimentally acquired 1D spectra (10A). The shifts from the simulation coalesce around 50ºC, and the chemical shift of the simulated averaged resonance at high temperature match with that of the experimentally observed signal before the interconverting duplexes melt to the single strand form.

ppm). This qualitatively indicates that there is a change in the conformation around residue $\underline{A}^6$ compared to native B-DNA structures with only very small changes in the structure of the sugar residues. The H8-H1' crosspeak of $\underline{A}^6$ (in italic font shown by an outlined arrow in Figure 8A) assigned to duplex (**1B**), has a much quicker NOE buildup (Figure 8B) than the corresponding resonance in the trace for duplex (**1A**) (plain font shown by a solid arrow in Figure 8A), indicating a possible syn conformation for the former. For the assignment trace for duplex (**1B**), in contrast with the trace for duplex (**1A**), there is a break in the usual aromatic-aromatic connectivity between $A^5$ and $A^6$. Instead, one observes a H8$A^5$ to H2$\underline{A}^6$ crosspeak (Figure 9). In normal B-type DNA conformation, the H8A5 to H8A6 distance is around 5.0Å , while it is around 9.4Å in a minimised model system when one of the bases is Hoogsteen basepaired. However, a similar model study showed that the H8$A^5$ to H2$\underline{A}^6$ distance is around 8.8 in Watson-Crick basepairing while it is only around 3.7 when one of the bases is Hoogsteen basepaired to the opposite strand. The observed NOE crosspeak between H8$A^5$ to H2$\underline{A}^6$ together with the NOE contacts found between imino proton H3 of $T^7$, H8$\underline{A}^6$ and H1'$\underline{A}^6$ convinced us that the two central basepairs in duplex (**1B**) are Hoogsteen basepaired.

**Table II.**

The North ⇄ South conformational equilibrium of each sugar residue was estimated using the equation %S = ( $J_{H1'}$ - 9.8) / 5.9 (*26*) for the Watson-Crick basepaired duplex (**1A**) and the Hoogsteen basepaired duplex (**1B**). The measurement error is estimated to 1, 2 and 3 Hz respectively for $J_{H1'}$, $J_{H2'}$ and $J_{H2''}$ (*25*) at 20 C for molecules of this size.

| Residue | Conformation | $J_{H1'}$ | $J_{H2'}$ | $J_{H2''}$ | South conformation |
|---|---|---|---|---|---|
| $C^1$ | * | 15.3 | 26.6 | 22.6 | 93% |
| $G^2$ | * | ‡ | ‡ | ‡ | |
| $C^3$ | 1A | 14.5 | 27.5 | 24.2 | 80% |
| $C^3$ | 1B | 14.5 | 28.3 | 24.2 | 80% |
| $G^4$ | 1A | 16.2 | 26.6 | 24.2 | 100% |
| $G^4$ | 1B | 17.8 | 26.6 | 23.4 | 100% |
| $A^5$ | 1A | 16.2 | ‡ | ‡ | 100% |
| $A^5$ | 1B | 15.3 | 26.6 | ‡ | 93% |
| $\underline{A}^6$ | 1A | ‡ | ‡ | ‡ | |
| $\underline{A}^6$ | 1B | ‡ | ‡ | ‡ | |
| $T^7$ | 1A | 14.5 | 29.1 | 25.8 | 80% |
| $T^7$ | 1B | 15.3 | 30.7 | 25.8 | 93% |
| $T^8$ | 1A | 16.9 | 29.9 | 25.0 | 100% |
| $T^8$ | 1B | 16.9 | 29.1 | 25.0 | 100% |
| $C^9$ | 1A | 15.3 | 27.5 | 21.8 | 93% |
| $C^9$ | 1B | 15.3 | 27.5 | 21.8 | 93% |
| $G^{10}$ | 1A | ‡ | ‡ | ‡ | |
| $G^{10}$ | 1B | ‡ | ‡ | ‡ | |
| $C^{11}$ | * | 14.5 | 25.8 | 25.8 | 80% |
| $G^{12}$ | * | 15.3 | 27.5 | 23.4 | 93% |

* The terminal residues ($C^1$, $G^2$, $C^{11}$ and $G^{12}$) have isochronous shifts for the duplexes (**1A**) and (**1B**).

‡ Residues $G^2$, $G^4$, $G^{10}$, and $\underline{A}^6$ and some $A^5$ peaks were not sufficiently resolved to determine coupling constants. However, the H1'-H2' coupling being stronger than the H1'-H2'' for all residues, except $\underline{A}^6$ which could not be estimated, indicates that all residues are in South conformation.

*(4) Hoogsteen basepairing*

Here follows a summary of our observations favouring Hoogsteen basepairing at the central two A-T basepairs in (**1B**). The big changes in the chemical shifts for the central $\underline{A}^6$ and $T^7$ residues (as well as for the neighbouring $A^5$ and $T^8$) indicates that there is a major change in base stacking at the centre of the duplex, which could not explained by a standard Watson-Crick basepaired B-type DNA duplex.

**Table III.**
Torsion constraints used in the calculations‡. No differences in torsions between the two different conformations could be established from the NMR data.

| Residue | | | | | | |
|---|---|---|---|---|---|---|
| $C^1$ | - | - | | 140±30 | 180±40 | 300±40 |
| $G^2$ | 300±40 | 180±40 | 60±40 | 140±30 | 180±40 | 300±40 |
| $C^3$ | 300±40 | 180±40 | 60±40 | 140±30 | 180±40 | 300±40 |
| $G^4$ | 300±40 | 180±40 | 60±40 | 140±30 | 180±40 | 300±40 |
| $A^5$ | 300±50 | 180±50 | 60±50 | 140±30 | 240±120 | 300±50 |
| $A^6$ | | | | | 240±120 | |
| $T^7$ | | | | 140±30 | 240±120 | |
| $T^8$ | | | | 140±30 | 180±50 | |
| $C^9$ | 300±40 | 180±40 | 60±40 | 140±30 | 180±40 | 300±40 |
| $G^{10}$ | 300±40 | 180±40 | 60±40 | 140±30 | 180±40 | 300±40 |
| $C^{11}$ | 300±40 | 180±40 | 60±40 | 140±30 | 180±40 | 300±40 |
| $G^{12}$ | 300±40 | 180±40 | 60±40 | 140±30 | - | - |

‡ In addition, the chi torsion in the Watson-Crick and Hoogsteen refinements were contrained to *anti* and *syn* respectively using hydrogen bond contraints for residue $A^6$-$T^7$. All other residues are Watson-Crick basepaired.
These torsions were not constrained.

That this is indeed owing to Hoogsteen basepairing is evident from the following observations: (i) Duplex (**1B**) has NOESY crosspeaks between $H3T^7$ and $H8\underline{A}^6$, $H3T^7$ and $H1'\underline{A}^6$ and between $H3T^8$ and $H8\underline{A}^6$ (Figure 6), which is consistent with what is expected from Hoogsteen basepairing (Figure 7), as found in the earlier base triple DNA (11). (ii) The H8-H1' crosspeak of $\underline{A}^6$ (in *italic* font shown by an outlined arrow in Figure 8A) assigned to duplex (**1B**), has a much quicker NOE buildup, with a 6-7 fold larger intensity at ca 70 ms mixing time, (Figure 8B) than the corresponding crosspeak in the fully Watson-Crick basepaired duplex (**1A**) (plain font shown by a solid arrow in Figure 8A), which suggests a *syn* conformation for the former (Figure 8B). (iii) The observed NOE crosspeak between $H8A^5$ to $H2\underline{A}^6$ and together with the interruption in the aromatic-aromatic connectivity between $A^5$ and $\underline{A}^6$, which is expected in normal B-type DNA, and is also found for (1A), indicates syn conformation (see above). (iv) Finally, we observe temperature-dependent exchange peaks in ROESY and NOESY spectra between the resonances belonging to duplexes (**1A**) and (**1B**), showing that the two conformers exist in a dynamic interconverting equilibrium.

Thus we concluded, along with the coalescence data shown below, that duplex (**1**) exists in two dynamically interconverting conformations: a fully Watson-Crick basepaired DNA duplex (**1A**) and a doubly $\underline{A}^6$:$T^7$ Hoogsteen basepaired (**1B**) B-type DNA duplex. A summary of proton chemical shifts for (**1A**) and (**1B**) can be found in Table 1.

*(5) Coalescence*

As mentioned above, at temperatures below 50ºC, the spectra of duplex (**1**) show two different sets of resonances for all protons of residues $C^3$, $G^4$, $A^5$, $\underline{A}^6$, $T^7$, $T^8$, $C^9$ and $G^{10}$ (Figures 5, 6, 8 and 9). The protons of the terminal $C^1$, $G^2$, $C^{11}$, $G^{12}$ residues are however not affected, each proton having only one set of resonances. ROESY spectra show chemical exchange crosspeaks between those sets of resonances (Figure 5B). Upon increasing the temperature, the two different sets of signals (shown only for two $MeT^7$ resonances) from two conformers (Figures 10A, C) start to move towards each other until they coalesce at ~320K. As the temperature is increased, the interconversion between (**1A**) and (**1B**) becomes faster in the NMR time scale, showing the average chemical shift at around 335K. When the

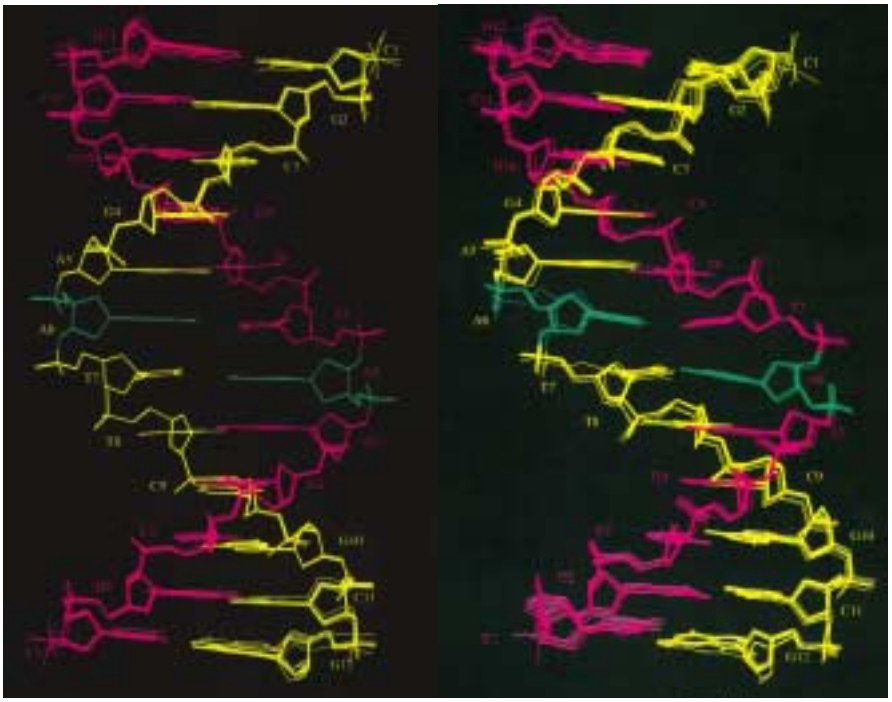

**Figure 11.** (A) Superimposition of 8 representative Watson-Crick basepaired duplex structures after the Step 2 refinement (**1A**) [RMSD = 0.33Å]. (B) Superimposition of 8 representative Hoogsteen basepaired duplex structures after the Step 2 refinement (**1B**) [RMSD = 0.38Å]. The modified residue, $\underline{A}^6$, is highlighted in green.

temperature is further increased, the duplex melts to single strand at a $T_m$ of 72ºC under NMR conditions (see materials and methods). Figure 10C also shows that the two sets of resonances from the two different conformers coalesce at the chemical shift predicted by the relative molar ratios (see materials and methods) of the two components found at temperatures below coalescence. Using rate constants extracted from the exchange calculations as well as the molar ratios, it has been possible to simulate (*19*) the coalescence appearance of the spectra (Figure 10B), thus further validating the fact that it is coalescence we are observing, and not a third conformation, for example a hairpin structure (*9*). This is also strengthened by the fact that the equilibrium between the two conformers does not significantly change by altering either concentration (5 to 200 o.d. at A254) or temperature (0-86ºC).

*(6) Sugar and backbone conformations*

From the DQF-COSY spectra, we could determine the sugar conformation: The $\Sigma J_{H1'}$ was used to estimate the %S conformation and was found to be predominantly of S-type [C2 -*endo*- C3 -*exo*; $110^o < P < 180^o$; $\Phi_m = 38 \pm 4^o$] conformation (Table 2) for all residues except $\underline{A}^6$, which could not be determined. The $\Sigma J_{H1'}$ (~15 Hz) has the lowest error (± 1 Hz) compared to $\Sigma J_{H2'}$ (27-30 Hz) and $\Sigma J_{H2"}$ (21-25 Hz; line-broadening as much as 3 Hz at 20ºC) (*26*). A comparison of these three groups of coupling constants suggests that the sugar conformations are locked mainly in S-type conformation. Though the sum rule (*27*) shows the % population of N- or S-type conformers, it is difficult to define any restrictions concerning the geometry. These considerations have led us to restrict the pentose conformer broadly in the S-type region in the NMR structure building protocol ($P = 160 \pm 25^o$; $\Phi = 38 \pm 4^o$) (*10a, 27*) in X-PLOR (14).

Using the procedures described by Chou et al (*28*) and Kim et al (*29*), we could constrain most of the other torsions of the sugar-phosphate backbone (Table 3). In a heteronuclear $^1H$-$^{31}P$ correlation spectrum, the (n)P-(n)H4' correlation is only detectable when the four bonds in the H4'-C4'-C5'-O5'-P backbone are located in the same plane forming a W-shaped conformation (*30*). This is possible when the β and γ torsion angles are *trans* and *gauche*$^+$ respectively, as in the case of B-DNA. The presence of observable (n)P-(n)H4' crosspeaks (data not shown) for residues 2-5 and 9-12 allowed us to constrain these residues to $\beta^t$ and $\gamma^+$. Additionally we could confirm the β and γ torsions using the linewidths of the NOESY crosspeaks

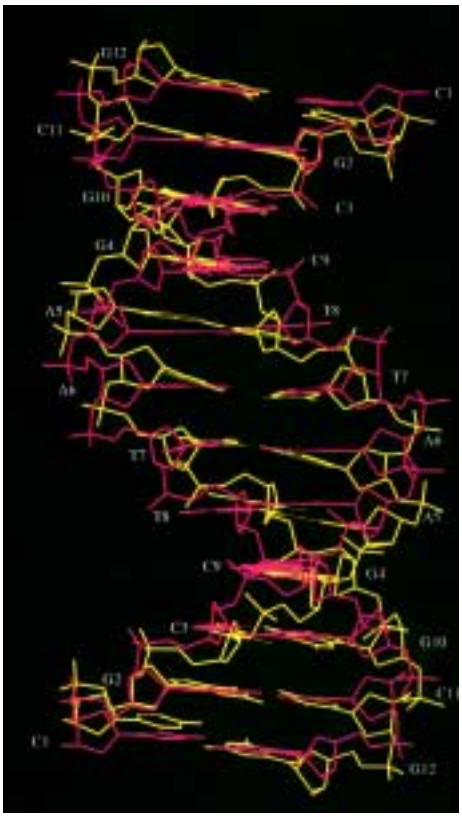

**Figure 14.** Superimposition of the final average structures for the Watson-Crick basepaired duplex (**1A**) (magenta) and the Hoogsteen basepaired duplex (**1B**) (yellow). The RMSD between the Watson-Crick structure and the Hoogsteen structure is ~1.5 Å (Table 4B).

**Table IV.**
The RMSD (Å) between the different structures

(a) The spread of RMSD by comparison of the accepted* (75 structures) Watson-Crick structures with their average structure, and of the (57 structures) Hoogsteen structures with their respective average structures, showing the diversity of the accepted structures.

| | Backbone atoms | | | Heavy atoms | | | All atoms | | |
|---|---|---|---|---|---|---|---|---|---|
| | all | $G^2$-$C^{11}$ | $A^5$-$T^8$ | All | $G^2$-$C^{11}$ | $A^5$-$T^8$ | all | $G^2$-$C^{11}$ | $A^5$-$T^8$ |
| Watson-Crick (**1A**) | 0.29 | 0.20 | 0.18 | 0.26 | 0.19 | 0.15 | 0.33 | 0.25 | 0.30 |
| Hoogsteen (**1B**) | 0.34 | 0.25 | 0.21 | 0.32 | 0.22 | 0.16 | 0.38 | 0.29 | 0.32 |

(b) RMSD between the average Watson-Crick structure (**1A**) and the average Hoogsteen structures (**1B**).

| Watson-Crick (**1A**) | Backbone atoms | | | Heavy atoms | | | All atoms | | |
|---|---|---|---|---|---|---|---|---|---|
| compared to: | All | $G^2$-$C^{11}$ | $A^5$-$T^8$ | all | $G^2$-$C^{11}$ | $A^5$-$T^8$ | all | $G^2$-$C^{11}$ | $A^5$-$T^8$ |
| Hoogsteen (**1B**) | 1.44 | 1.48 | 1.56 | 1.39 | 1.42 | 1.73 | 1.46 | 1.49 | 1.87 |

(c) RMSD between the average final structures of (**1A**) and (**1B**) and a standard Arnott's B-DNA construct‡ of the native Dickerson-Drew dodecamer [5'-(CGCGAATTCGCG)-3']$_2$.

| | Backbone atoms | | | Heavy atoms | | | All atoms | | |
|---|---|---|---|---|---|---|---|---|---|
| | All | $G^2$-$C^{11}$ | $A^5$-$T^8$ | all | $G^2$-$C^{11}$ | $A^5$-$T^8$ | all | $G^2$-$C^{11}$ | $A^5$-$T^8$ |
| Watson-Crick (**1A**) | 1.15 | 0.91 | 0.37 | 1.16 | 1.01 | 0.64 | 1.26 | 1.11 | 0.74 |
| Hoogsteen (**1B**) | 1.60 | 1.38 | 1.06 | 1.61 | 1.42 | 1.16 | 1.74 | 1.53 | 1.29 |

(d) RMSD between the average structures of (**1A**) and (**1B**) and the NMR structure (*4*) of the native Dickerson-Drew dodecamer (**2**).

| | Backbone atoms | | | Heavy atoms | | | All atoms | | |
|---|---|---|---|---|---|---|---|---|---|
| | all | $G^2$-$C^{11}$ | $A^5$-$T^8$ | all | $G^2$-$C^{11}$ | $A^5$-$T^8$ | all | $G^2$-$C^{11}$ | $A^5$-$T^8$ |
| Watson-Crick (**1A**) | 2.61 | 2.25 | 0.98 | 2.06 | 1.87 | 0.97 | 2.20 | 1.93 | 1.09 |
| Hoogsteen (**1B**) | 2.42 | 2.10 | 1.29 | 1.94 | 1.76 | 1.15 | 2.09 | 1.82 | 1.29 |

of H6/H8 to H4' (29) for these residues, but did not lead to any tighter constraints. For the central $\underline{A}^6$, $T^7$, $T^8$ residues, the overlap of resonances prevented the measurement of linewidths.

If ε is in *gauche*$^-$ conformation it should produce a detectable $^4J_{H2',P}$ coupling, while if ε is in *trans* conformation no significant $^4J_{H2',P}$ will be observable (*28*). Thus, the absence of crosspeaks in a $^1H$-$^{31}P$ correlation spectrum allowed us to rule out ε$^-$ for $C^1$, $G^2$, $C^3$, $G^4$, $T^8$, $C^9$, $G^{10}$ and $C^{11}$ residues, thereby constraining them

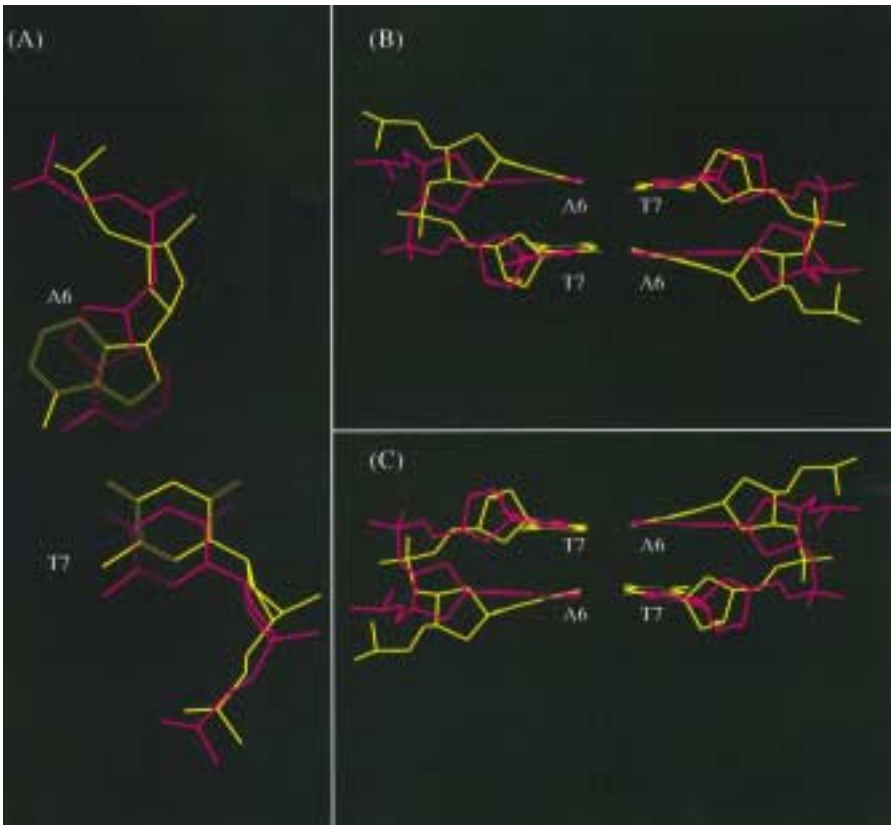


**Figure 15.** A zoom of the central A-T basepair (Watson-Crick: magenta, Hoogsteen: yellow) seen from above (A) and from the minor groove (B).

to the *trans* conformation (B1-type) since *gauche*$^+$ appears to be sterically forbidden (*10a,27*). For the other residues, we allowed both *trans* and *gauche*$^-$, only for-

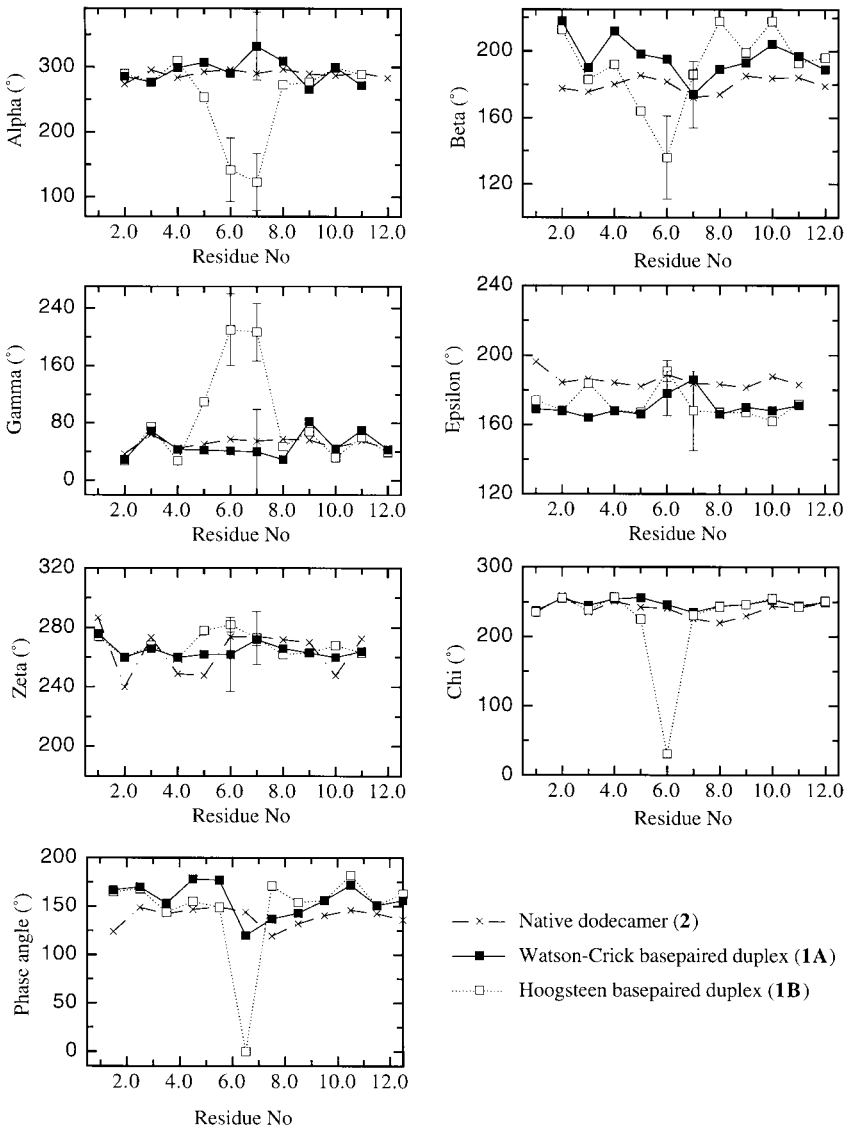


**Figure 12.** Comparison of the backbone torsions of the final average structures between the natural duplex (2) (*4*) and the two duplex structures (**1A** and **1B**) containing 2'-deoxyaristeromycin. Error bars have been added to the two central residues A6 and T7. The standard deviations of all other residues are less than 5°.

bidding *gauche*$^+$.

For ζ and α we used the qualitative $^{31}$P chemical shifts argument (*30a*) (from inverse $^1$H-$^{31}$P-correlation spectra at 20ºC) to exclude the trans domain. A ζ$^-$/α$^-$ conformation will have a relatively more upfield chemical shift (30a) than either zt/a- or z-/at torsions. As all our chemical shifts for residues G$^2$-A$^5$ and C$^9$-G$^{12}$ were in the normal range as for the native Dickerson's 12mer duplex (**2**) (*4*), *i.e.* from -3.7 to -4.1 ppm at 20ºC (Table 1), we concluded that gauche-gauche phosphate ester conformations prevail in both (**1A**) and (**1B**) over the trans conformations (*4, 15, 31*). However, since we are unaware of how the absence of the electronegative O4' in 2'-deoxyaristeromycin moiety affects the $^{31}$P chemical shift, we decided not to constrain the α and ζ of either $\underline{A}^6$ residue or its basepairing partner, T$^7$. Due to the lack of other backbone constraints for residue T$^8$, and the slight downfield shift (0.14 ppm) compared to the native duplex (**2**), we did not wish to use the $^{31}$P chemical shifts derived α/ζ constraint alone for this residue. Additionally, we allowed slightly larger ranges (Table 3) for the torsion angles close to residue $\underline{A}^6$ to ensure that we did not impose any bias by applying conventional rules coming from natural DNA/RNA to our carbocyclic residue.

Interestingly, the NMR derived backbone torsion constraints were all found to have the same ranges for both the Watson-Crick and the Hoogsteen structures. A sum

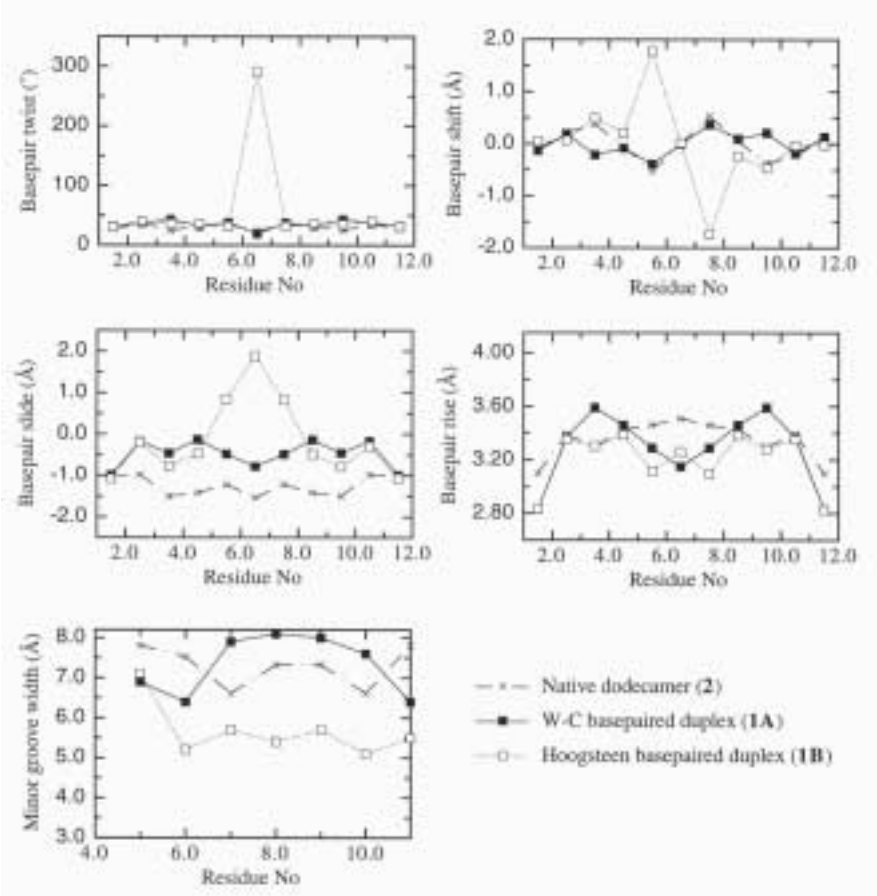


**Figure 13.** Comparison of some helical parameters of the final average structures between the natural duplex (**2**) (*4*) structure and the two duplex structures (**1A** and **1B**) containing 2'-deoxyaristeromycin (**1**).

mary of our torsion angle constraints is given in Table 3.

*(7) Constraints*

*Step 1:* After integration of NOE crosspeaks (35, 70 and 150 ms) by the AURELIA program (*20*), the calculated volumes were translated into internuclear distances using the two-proton approximation on crosspeaks from the 35 and, when neces-

**Table V.**
The backbone torsions (deg) of the average structures[‡]: Watson-Crick basepaired structures (**1A**), Hoogsteen basepaired structures (**1B**) after the *Step 2* refinements and Native duplex structure (**2**)[*].

| Duplex | Torsion | C[6] | G[2] | C[3] | G[4] | A[5] | A[6] | T[7] | T[8] | C[9] | G[10] | C[11] | G |
|---|---|---|---|---|---|---|---|---|---|---|---|---|---|
| (**1A**) | | - | 286 | 277 | 299 | 307 | 291 | 332 | 309 | 266 | 299 | 272 | |
| (**1B**) | | - | 290 | 277 | 310 | 254 | 142 | 123 | 273 | 277 | 299 | 289 | |
| (**2**) | | - | 275 | 295 | 283 | 293 | 293 | 291 | 296 | 290 | 289 | 291 | 2 |
| (**1A**) | | - | 218 | 190 | 212 | 198 | 195 | 174 | 190 | 193 | 204 | 197 | 1 |
| (**1B**) | | - | 213 | 183 | 192 | 164 | 136 | 186 | 218 | 199 | 218 | 193 | 1 |
| (**2**) | | - | 175 | 177 | 181 | 186 | 183 | 174 | 174 | 185 | 182 | 182 | 1 |
| (**1A**) | | - | 29 | 69 | 43 | 42 | 41 | 40 | 29 | 82 | 44 | 70 | 4 |
| (**1B**) | | - | 27 | 76 | 27 | 110 | 210 | 207 | 47 | 68 | 32 | 60 | 3 |
| | | - | 38 | 64 | 45 | 52 | 55 | 59 | 56 | 57 | 45 | 56 | 4 |
| (**1A**) | | 144 | 146 | 138 | 146 | 146 | 118 | 125 | 127 | 141 | 144 | 134 | 1 |
| (**1B**) | | 144 | 145 | 132 | 137 | 144 | 110 | 153 | 137 | 142 | 150 | 134 | 1 |
| (**2**) | | | | | | | | | | | | | |
| (**1A**) | | 169 | 168 | 164 | 168 | 166 | 178 | 186 | 166 | 170 | 168 | 171 | |
| (**1B**) | | 174 | 168 | 184 | 168 | 167 | 191 | 168 | 167 | 167 | 162 | 172 | |
| (**2**) | | 195 | 180 | 187 | 182 | 182 | 188 | 186 | 184 | 183 | 188 | 184 | |
| (**1A**) | | 276 | 260 | 266 | 260 | 262 | 262 | 273 | 266 | 264 | 260 | 264 | |
| (**1B**) | | 274 | 260 | 268 | 259 | 278 | 282 | 273 | 262 | 263 | 268 | 263 | |
| (**2**) | | 287 | 249 | 274 | 251 | 251 | 267 | 275 | 271 | 272 | 248 | 273 | |

sary, 70 ms spectra, with H5-H6 as reference distance (2.45 ). An error margin of ± 0.5Å was used as constraint. Another 0.5Å were added to the upper limit of NOEs involving methyl protons. NOEs that could not be integrated were classified into 5 ranges: 1.8-2.5Å , 1.8-3.0Å , 1.8-3.5Å , 2.3-5.0Å and 3.5-6.0Å corresponding to very strong, strong, medium, weak and very weak NOEs respectively.

For the Watson-Crick structure a total of 127 intra, 97 inter and 17 cross-strand dis-

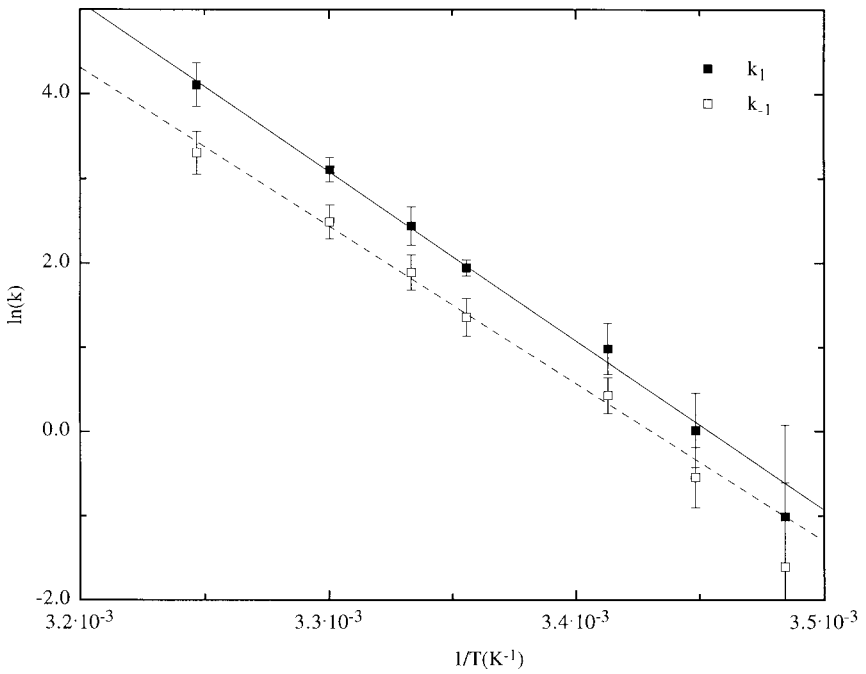


**Figure 16.** Arrhenius plot of the rate constants $k_1$ and $k_{-1}$ determined by a combination of ROESY/NOESY experiments at various mixing times and temperatures. The slope gives the energy of activation, $E_a$, which gives the contributions of enthalpy, $\Delta H^{o\ddagger}$, and entropy, $\Delta S^{o\ddagger}$, of activation.

tance constraints were used per strand. For the Hoogsteen structure we obtained 114 intra, 92 inter and 15 cross-strand distance constraints. This gives an average of 22 and 20 NOE distance constraints per residue and strand, in addition to the 55 backbone dihedral constraints per strand (see sugar and backbone conformation), for the Watson-Crick and Hoogsteen structures respectively. The number of contraints are summarised in Figure 3. All NMR-observed basepaired residues were kept basepaired by hydrogen-bonding constraints.

Since all sugar residues were found to be in the S-type conformation, we have modelled C2 -*endo* conformation with sugar pucker constraints using dihedrals, $\nu 0$, $\nu_1$, $\nu_2$, $\nu_3$ and $\nu_4$, to set to the phase angle to 160 ± 25°, $\Phi$ = 38  4° except for the central $\underline{A}^6$ residue which was not constrained. The following sugar-phosphate torsion constraints were also used (see discussion above): The $\alpha$ and $\zeta$ torsions were excluded from the trans domain. $\beta$ torsions are constrained to $\beta^t$. Gamma torsions are constrained to $\gamma^+$. $\varepsilon$ torsions were constrained to et domain for the non-central residues and only excluded from $\varepsilon^+$ for the central ones, resulting in a total of 55 dihedral constraints. Thus, we could partly constrain the backbone torsions (Table 3) except for those of residues $\underline{A}^6$, $T^7$ and $T^8$.

*Step 2:* 175 of the crosspeaks used in the step 1 calculation could be integrated satisfactory at all three mixing times (35, 70 and 150 ms). These crosspeaks were run through three cycles of MARDIGRAS/RANDMARDI/X-PLOR (14, 17) using 10 accepted low-energy structures from the *Step 1* calculations as input structures in RANDMARDI. Methyl jump model 3 and absolute unnormalised noise of the same magnitude as the smallest peaks in the spectra were used and the error margin was never allowed to be smaller than ± 0.5Å. A hybrid between the resulting NOE constraints and the NOE constraints from the first calculation was then used to refine the final *Step 2* structures. The same dihedral constraints as those in the *Step 1* calculation were applied to the *Step 2* refinement.

All NOE connections are shown in Figure 2. All NMR observed constraints used for structure calculation are shown in Table 3, and Figures 2 and 3.

*(8) Refinement and analysis of the final structures*

We have calculated NMR constrained structures for both the Watson-Crick and the Hoogsteen basepaired conformations. From anti-parallel A- and B-DNA constructs

**Table VI.**
Helical parameters of the final structures.

(a) The intra basepair helical parameters of the Watson-Crick (**1A**) and the Hoogsteen (**1B**) basepaired structures after the *Step 2* refinement compared to the NMR structure (*4*) of the native Dickerson-Drew Dodecamer (**2**). The modified basepairs ($\underline{A}^6$-$T^7$ and $T^7$-$\underline{A}^6$) have been shaded.

| Basepair | Duplex | Buckle | Propeller | Open | Shear | Stretch | Stagger |
|---|---|---|---|---|---|---|---|
| $C^1$-$G^{12}$ | (**1A**) | -0.1 | -1.1 | 4.5 | -0.4 | 0.2 | 0.1 |
| | (**1B**) | 0.0 | -0.6 | 4.4 | 0.1 | 0.1 | 0.0 |
| | (**2**) | 2.1 | -23.6 | 7.8 | 0.6 | 0.1 | -0.2 |
| $G^2$-$C^{11}$ | (**1A**) | 1.6 | 1.9 | 4.5 | -1.1 | -0.1 | 0.1 |
| | (**1B**) | 0.0 | -0.2 | 4.6 | -1.0 | -0.1 | 0.0 |
| | (**2**) | -0.6 | -0.5 | 2.7 | 0.1 | 0.2 | 0.4 |
| $C^3$-$G^{10}$ | (**1A**) | -0.4 | -0.4 | 5.8 | -0.7 | 0.3 | -0.3 |
| | (**1B**) | 0.1 | 1.3 | 5.1 | 0.5 | 0.1 | -0.1 |
| | (**2**) | -5.9 | -0.6 | 3.8 | 0.6 | 0.1 | 0.3 |
| $G^4$-$C^9$ | (**1A**) | -5.5 | 3.2 | 3.3 | 0.9 | 0.3 | 0.1 |
| | (**1B**) | -0.7 | -0.6 | 4.8 | 0.8 | 0.3 | 0.0 |
| | (**2**) | 4.2 | 11.5 | 5.5 | -0.2 | 0.2 | -0.1 |
| $A^5$-$T^8$ | (**1A**) | -3.2 | -1.9 | 5.8 | 0.3 | 0.3 | 0.1 |
| | (**1B**) | -1.2 | -0.3 | 3.8 | 1.4 | 0.1 | -0.5 |
| | (**2**) | 1.5 | 8.0 | 3.0 | 0.0 | 0.2 | -0.5 |
| $\underline{A}^6$-$T^7$ | (**1A**) | -5.2 | -7.4 | 5.2 | 1.2 | 0.1 | -0.5 |
| | (**1B**) | 120.5 | -110.7 | 15.5 | -0.4 | -3.8 | -4.1 |
| | (**2**) | 6.7 | -4.0 | 1.0 | 0.2 | 0.2 | -0.2 |
| $T^7$-$\underline{A}^6$ | (**1A**) | 5.5 | -5.9 | 5.1 | -1.2 | 0.1 | -0.5 |
| | (**1B**) | -121.5 | -110.7 | 15.0 | 0.4 | -3.8 | -4.2 |
| | (**2**) | -6.7 | -4.0 | 1.0 | -0.2 | 0.2 | -0.2 |
| $T^8$-$A^5$ | (**1A**) | 3.3 | -1.6 | 4.6 | -0.3 | 0.3 | 0.1 |
| | (**1B**) | 1.2 | -0.7 | 3.9 | -1.4 | 0.1 | -0.5 |
| | (**2**) | -1.5 | 8.0 | 3.0 | 0.0 | 0.2 | -0.5 |
| $C^9$-$G^4$ | (**1A**) | 5.1 | 3.2 | 3.6 | -0.9 | 0.3 | -0.1 |
| | (**1B**) | 0.3 | -0.9 | 4.8 | -0.8 | 0.3 | 0.1 |
| | (**2**) | -4.2 | 11.5 | 5.5 | 0.2 | 0.2 | -0.1 |
| $G^{10}$-$C^3$ | (**1A**) | 0.6 | -0.3 | 5.8 | 0.7 | 0.3 | 0.0 |
| | (**1B**) | 0.3 | 1.3 | 5.0 | -0.6 | 0.1 | -0.1 |
| | (**2**) | 5.9 | -0.5 | 3.8 | -0.6 | 0.1 | 0.3 |
| $C^{11}$-$G^2$ | (**1A**) | -1.3 | 2.0 | 4.5 | 1.1 | -0.1 | 0.1 |
| | (**1B**) | -0.2 | -0.1 | 4.4 | 1.0 | -0.1 | 0.0 |
| | (**2**) | 0.6 | -0.5 | 2.7 | -0.1 | 0.2 | 0.4 |
| $G^{12}$-$C^1$ | (**1A**) | 0.0 | -1.1 | 4.5 | 0.4 | -0.1 | 0.1 |
| | (**1B**) | 0.0 | -0.5 | 4.4 | -0.1 | 0.1 | 0.0 |
| | (**2**) | -2.1 | -23.7 | 7.8 | -0.6 | 0.1 | -0.2 |

(b) The inter basepair helical parameters of the Watson-Crick (1A) and the Hoogsteen (1B) basepaired structures. The basepairs involved in the Hoogsteen basepairing in duplex (**1B**) ($\underline{A}^6$-$T^7$ and $T^7$-$\underline{A}^6$) have been shaded.

| From to | Duplex | Tilt | Roll | Twist | Shift | Slide | Rise | Incl | Tip | Dx | Dy | Dz |
|---|---|---|---|---|---|---|---|---|---|---|---|---|
| $C^1$ $G^2$ | (**1A**) | -3.2 | 5.4 | 31.9 | -0.1 | -1.0 | 2.8 | 9.6 | 5.8 | -2.6 | -0.3 | 2.6 |
| | (**1B**) | -0.3 | 5.6 | 30.9 | 0.0 | -1.1 | 2.8 | 10.4 | 0.6 | -2.9 | -0.1 | 2.6 |
| | (**2**) | -5.2 | 13.3 | 26.2 | -0.1 | -1.0 | 3.1 | 26.6 | 10.3 | -4.4 | -0.8 | 2.3 |
| $G^2$ $C^3$ | (**1A**) | 0.4 | 4.8 | 37.0 | 0.2 | -0.2 | 3.4 | 7.3 | -0.5 | -0.9 | -0.2 | 3.3 |
| | (**1B**) | 1.1 | -0.9 | 40.4 | 0.1 | -0.2 | 3.4 | -1.3 | -1.5 | -0.2 | 0.0 | 3.4 |
| | (**2**) | 1.2 | 10.9 | 36.8 | 0.2 | -1.0 | 3.4 | 16.6 | -1.8 | -2.9 | -0.2 | 3.0 |
| $C^3$ $G^4$ | (**1A**) | 0.8 | -0.4 | 43.3 | -0.2 | -0.5 | 3.6 | -0.5 | -1.0 | -0.6 | 0.4 | 3.6 |
| | (**1B**) | 4.4 | 5.5 | 36.1 | 0.5 | -0.8 | 3.3 | 8.7 | -6.9 | -2.0 | -0.2 | 3.2 |
| | (**2**) | 2.0 | -3.9 | 24.3 | 0.4 | -1.5 | 3.3 | -9.1 | -4.6 | -2.2 | -0.2 | 3.5 |
| $G^4$ $A^5$ | (**1A**) | -3.1 | 3.2 | 32.1 | -0.1 | -0.1 | 3.5 | 5.6 | 5.4 | -0.8 | -0.4 | 3.4 |
| | (**1B**) | 2.6 | -1.3 | 36.6 | 0.2 | -0.5 | 3.4 | -2.0 | -4.0 | -0.6 | 0.0 | 3.4 |
| | (**2**) | 2.2 | 9.9 | 33.3 | 0.0 | -1.4 | 3.4 | 16.6 | -3.6 | -3.9 | 0.4 | 2.9 |
| $A^5$ $\underline{A}^6$ | (**1A**) | 0.3 | 3.0 | 38.0 | -0.4 | -0.5 | 3.3 | 4.4 | -0.5 | -1.1 | 0.6 | 3.2 |
| | (**1B**) | 85.9 | -34.2 | 31.8 | 1.8 | 0.8 | 3.1 | -26.2 | -65.9 | 1.5 | 1.2 | 2.3 |
| | (**2**) | -0.9 | -6.2 | 33.9 | -0.5 | -1.2 | 3.5 | 10.3 | 1.5 | -1.0 | 0.7 | 3.6 |
| $\underline{A}^6$ $T^7$ | (**1A**) | -0.3 | -1.4 | 19.1 | 0.0 | -0.8 | 3.2 | -4.1 | 1.0 | -1.7 | -0.1 | 3.2 |
| | (**1B**) | 0.1 | 103.9 | -69.6 | 0.0 | 1.9 | 3.3 | -56.2 | 0.0 | -2.1 | 0.0 | 0.2 |
| | (**2**) | 0.0 | 2.2 | 24.5 | 0.0 | -1.5 | 3.5 | 5.1 | 0.0 | -4.3 | 0.0 | 3.4 |
| $T^7$ $T^8$ | (**1A**) | -0.1 | 3.1 | 37.3 | 0.4 | -0.5 | 3.3 | 4.8 | 0.1 | -1.2 | -0.6 | 3.2 |
| | (**1B**) | -86.1 | -34.7 | 32.0 | -1.7 | 0.8 | 3.1 | -26.5 | 65.8 | 1.5 | -1.2 | 2.2 |
| | (**2**) | 0.9 | -6.2 | 33.9 | 0.5 | -1.2 | 3.5 | -10.3 | -1.5 | -1.0 | -0.7 | 3.6 |
| $T^8$ $C^9$ | (**1A**) | 2.6 | 3.0 | 32.7 | 0.1 | -0.1 | 3.5 | 5.2 | -4.6 | -0.8 | 0.3 | 3.4 |
| | (**1B**) | -2.3 | -1.6 | 36.5 | -0.2 | -0.5 | 3.4 | -2.6 | 3.7 | -0.5 | 0.0 | 3.4 |
| | (**2**) | -2.2 | 9.9 | 33.3 | 0.0 | -1.4 | 3.4 | 16.6 | 3.6 | -3.9 | -0.4 | 2.9 |
| $C^9$ $G^{10}$ | (**1A**) | -0.8 | -0.6 | 43.3 | 0.2 | -0.5 | 3.6 | -0.8 | 1.0 | -0.6 | -0.4 | 3.6 |
| | (**1B**) | -4.5 | 5.9 | 35.1 | -0.5 | -0.8 | 3.3 | 9.5 | 7.2 | -2.1 | 0.1 | 3.1 |
| | (**2**) | -2.0 | -3.9 | 24.3 | -0.4 | -1.5 | 3.3 | -9.1 | 4.6 | -2.2 | 0.2 | 3.5 |
| $G^{10}$ $C^{11}$ | (**1A**) | -0.3 | 4.5 | 37.0 | -0.2 | -0.2 | 3.4 | 6.9 | 0.5 | -0.9 | 0.2 | 3.3 |
| | (**1B**) | -1.1 | -2.2 | 40.1 | 0.0 | -0.3 | 3.4 | -3.1 | 1.6 | -0.2 | -0.1 | 3.4 |
| | (**2**) | -1.2 | 10.9 | 26.8 | -0.2 | -1.0 | 3.4 | 16.6 | 1.8 | -2.9 | 0.2 | 3.0 |
| $C^{11}$ $G^{12}$ | (**1A**) | 3.4 | 5.7 | 31.9 | 0.1 | -1.0 | 2.8 | 10.1 | -6.0 | -2.6 | 0.3 | 2.6 |
| | (**1B**) | 0.7 | 5.5 | 31.0 | 0.0 | -1.1 | 2.8 | 10.0 | -1.2 | -2.8 | 0.2 | 2.6 |
| | (**2**) | 5.2 | 13.3 | 26.3 | 0.1 | -1.0 | 3.1 | 26.6 | -10.3 | -4.4 | 0.8 | 2.3 |

(using SYBYL [*32*] based on Arnott's A- and B-DNA [*10b*]), 50 structures were

generated from each of the starting structures using a simulated annealing protocol (*16*). Thus, 100 structures for each duplex (**1A** and **1B**) were calculated using NMR constraints for either the Watson-Crick or the Hoogsteen basepaired conformations. Each structure was then refined in two steps using X-PLOR (*14*) protocols (see materials and methods).

*Step 1:* In the 100 calculations, 86 converged for the Watson-Crick structure and 72

**Table VII.**

(A) R-factor analysis comparing the Watson-Crick (**1A**) and Hoogsteen (**1B**) basepaired structures from the *Step 1* refinement to the corresponding NOE intensities using the density matrix program MARDIGRAS (*16*).

| | Watson-Crick (**1A**) (68 stuctures) | Hoogsteen (**1B**) (53 structures) |
|---|---|---|
| R | 0.67 ± 0.014 | 0.72 ± 0.024 |
| $R_2$ | 0.88 ± 0.028 | 0.93 ± 0.042 |
| $R^x$ | 0.16 ± 0.0053 | 0.17 ± 0.0053 |
| $R^x_2$ | 0.22 ± 0.0092 | 0.24 ± 0.0099 |

(B) R-factor analysis comparing the Watson-Crick (**1A**) and Hoogsteen (**1B**) basepaired structures from the *Step 2* refinement to the corresponding NOE intensities using the full relaxation matrix program MARDIGRAS (*16*).

| | Watson-Crick (**1A**) (86 stuctures) | Hoogsteen (**1B**) (64 structures) |
|---|---|---|
| R | 0.50 ± 0.055 | 0.53 ± 0.055 |
| $R_2$ | 0.59 ± 0.047 | 0.58 ± 0.052 |
| $R^x$ | 0.091 ± 0.012 | 0.098 ± 0.0061 |
| $R^x_2$ | 0.11 ± 0.014 | 0.12 ± 0.0061 |

for the Hoogsteen structure. These structures were harvested on the basis of violations of the NMR constraints used (see materials and methods section for the acceptance criteria). These structures were further screened on the basis of total energies in such a manner that no structure with a total energy more than 15 kcal higher than the lowest energy structure was accepted as a final structure. This left us with 68 Watson-Crick- (RMSD = 0.52Å) and 53 Hoogsteen basepaired structures (RMSD = 0.47Å).

*Step 2:* The convergence rate in the refinement using the RANDMARDI derived constraints was 86 out of 100 and 64 out of 100 for the Watson-Crick structure and the Hoogsteen structure, respectively, using the same structure harvesting procedure as in *Step 1*. The refined structures after *Step 2* were somewhat better defined than after *Step 1*: Watson-Crick structures (RMSD = 0.29Å, Table 4A, Figure 11A) and Hoogsteen structures (RMSD = 0.34Å, Table 4A, Figure 11B). The *Step 2* average Watson-Crick structure has an RMSD of 1.15 compared to a standard B-DNA construct (using SYBYL [*32*] based on Arnott's B-DNA [*10b*]), and the average of the Hoogsteen structures has an RMSD of 1.6Å (Table 4C). Compared to a NMR-derived model (4) of the native Dickerson-Drew dodecamer, both the Watson-Crick and the Hoogsteen structures have RMSDs of ~2.5Å (Table 4D).

The RMSD between the average final structures of the *Step 1* and *Step 2* calculations between 1.0 and 1.5Å for both the Watson-Crick basepaired duplex (**1A**) and the Hoogsteen basepaired duplex (**1B**). There are no major differences in either torsions or helical parameters (data not shown) between the two calculations for neither the Watson-Crick nor the Hoogsteen basepaired structures.

The NOE intensities were compared to the calculated structures, using complete relaxation matrix implemented by MARDIGRAS (*17*), for both the Watson-Crick and the Hoogsteen basepaired structures. The R-factors decrease by ~20% when going from *Step 1* to *Step 2* as a result of the MARDIGRAS/RANDMARDI treatment of the NOE constraints. The average R-factors are summarised in Table 7.

The average final structures of the Watson-Crick basepaired duplex and the Hoogsteen basepaired duplexes are superimposed in Figure 14 and a zoom of the

central A-T basepair of the same structures are displayed in Figure 15.

The Watson-Crick basepaired structure shows typical B-DNA like conformation (*4,10*). The largest deviations of the Hoogsteen structures from B-DNA are in a for $\underline{A}^6$, $T^7$ and $T^8$, γ for $\underline{A}^6$, $T^7$ and $T^8$ and δ for $\underline{A}^6$ (Figure 12 and Table 5). Some of these differences could however be caused by our lack of restraints for the sugar-phosphate backbone in the centre of the duplex.

In the Hoogsteen basepaired structures, the torsions differed in the following manner: The δ of $\underline{A}^6$ is between 92° and 111° instead of 120° to 150° as would be expected in typical B-DNA (*10*). The β torsions of $\underline{A}^6$ and $T^8$ show variations but are still in *trans*. The a torsion of $\underline{A}^6$ and $T^7$ are in the trans region instead of *gauche*$^-$ and γ of $\underline{A}^6$ and $T^7$ are in *trans* instead of *gauche*$^+$. In the *Step 1* calculations, both α and γ of residue $T^8$ can also be in trans but this alternative conformation is not seen in the *Step 2* structures. All torsions are summarised in Table 5.

The RMSD between the Watson-Crick structures and the Hoogsteen structures is also largest between the 4 central basepairs, *i.e*. residues $A^5$ to $T^8$. This shows that relatively few changes in torsion angles are enough to enable the bases of the 2 central residues to form Hoogsteen basepairs. Clearly, the facile *anti*⇄*syn* conversion in the carbocyclic $\underline{A}^6$ nucleotide moiety is promoted by the absence of the steric clash between the adenine-9-yl moiety and the high energy O4'-endo conformation found in natural 2'-deoxyribose (O4'-*endo* conformation in the pseudorotational path renders a high energy barrier [2.5 – 5 kcal/mol] between the low energy C2'-*endo* and C3'-*endo* conformations) (*33*).

A comparison of the helical parameters show large deviations of the partly Hoogsteen basepaired structure (**1B**) (two central $\underline{A}^6$ in *syn* conformation) from the native dodecamer (**2**). The affected helical parameters are: buckle, propeller, open, tilt, roll, twist, inclination and tip. Minor changes occur in stretch, stagger, slide and rise. On the other hand, there are no significant differences found between the fully Watson-Crick basepaired structure (**1A**) (Figures 12 and 13), with all residues in *anti* conformation, and the native counterpart. All helical parameters are given in Table 6.

For the $\underline{A}^6$-$T^7$ basepair, the buckle of the Hoogsteen basepaired structure (**1B**) increases by 125° compared to the Watson-Crick basepaired structure (**1A**). The propeller decreases by 115° and the open increases by 10°. Stretch and stagger decrease with 3-4°. Between basepair 5 ($A^5$-$T^8$) and 6 ($\underline{A}^6$-$T^7$) the tilt increases by 85°, the roll decreases by 30° and the inclination decreases by 25°. Between the two central basepairs 6 ($\underline{A}^6$-$T^7$) and 7 ($T^7$-$\underline{A}^6$) the roll increases by 105°, the twist decreases by 90° and the inclination decreases by 65° for the Hoogsteen basepair compared to the Watson-Crick basepair. The changes in basepair 7 ($T^7$-$\underline{A}^6$) and between 7 ($T^7$-$\underline{A}^6$) and 8 ($T^8$-$A^5$) are the same as for 6 ($\underline{A}^6$-$T^7$) and between 5 ($A^5$-$T^8$) and 6 ($\underline{A}^6$-$T^7$), respectively, for symmetrical reasons. The changes in the helical parameters mentioned above are caused by the two central residues ($\underline{A}^6$-$T^7$) being Hoogsteen basepaired, causing a disturbance in the base stacking which is also confirmed by abnormal chemical shifts for the set of resonances belonging to the Hoogsteen basepaired duplex (**1B**) (see above). The result of these changes on the overall structure is a narrowing of approximately 2-3Å of the minor groove (Figures 12 and 13) and a corresponding widening of the major groove.

*(9) Kinetics and thermodynamics*

We have also investigated the kinetics and thermodynamics of the exchange process: Watson-Crick basepairing (**1A**)⇄ Hoogsteen baseparing (**1B**), and the thermodynamics of the melting of the duplex. We have described above that the two sets of resonances for the two duplexes coalesce at ~50°C. From a set of temperature-dependent NOESY/ROESY spectra at 7 different mixing times (between

20 and 400 ms), it has been possible to extract the temperature-dependent rates ($k_1$ and $k_{-1}$) of the exchange process, giving the energy of activation (Ea) of the transition of both in the forward ($k_1$) ($E_a$ = 167 ± 14 kJ/mol) and reverse ($k_{-1}$) (Ea = 155 ± 13 kJ/mol) direction in [(**1A**)⇄ (**1B**)], using the Arrhenius equation (Figure 16) (See experimentals section for details). The ratio between $k_1$ and $k_{-1}$ is constant: $K_{eq} = k_1/k_{-1}$ = 0.56 ± 0.08. For the conversion of the Watson-Crick to the Hoogsteen, the $\Delta H^{o\ddagger}$ (298 K) is 164±14 kJ/mol and $-T\Delta S^{o\ddagger}$ (298 K) is -92 kJ/mol giving $\Delta G^{o\ddagger}_{298}$ of 72 kJ/mol. For the Hoogsteen to the Watson-Crick, the $\Delta H^{o\ddagger}$ (298 K) is 153±13 kJ/mol and $-T\Delta S^{o\ddagger}$ (298 K) is -82 kJ/mol giving $\Delta G^{o\ddagger}_{298}$ of 71 kJ/mol. The Gibbs free energy derived from the molar ratios at equilibrium, $\Delta G^{o\ddagger}_{298}$, is 1.4 kJ/mol to be compared to the $\Delta G^{o\ddagger}_{298}$ of approximately 1 kJ/mol. This shows that the energetic preference for one Watson-Crick basepair over one Hoogsteen basepair is relatively low (*i.e.* <0.7 kJ/mol/basepair) giving an equilibrium ratio of almost 2:1 in buffered aqueous solution.

The 2'-deoxyaristeromycin modified duplex, (**1**), has its melting point (by UV), $T_m$ = 65.2ºC, reduced by 2.4º compared to the native counterpart (2), $T_m$ = 67.6ºC. For the melting of the modified duplex (1) the $\Delta H^o$ is 314±6 kJ/mol and $-T\Delta S^o$ 271±5 kJ/mol giving a $\Delta G^{o\ddagger}_{298}$ of 43±8 kJ/mol. For the native counterpart (**2**), the $\Delta H^o$ is 319±8 kJ/mol and $-T\Delta S^o$ 274±6 kJ/mol giving a $\Delta G^{o\ddagger}_{298}$ of 45±10 kJ/mol.

***Conclusion***

A small change in one sugar residue (the O4' oxygen replaced by CH2) has been shown to have a dramatic effect on the local structure and flexibility of a B-type DNA duplex. The duplex is in an equilibrium between a typical fully Watson-Crick basepaired B-DNA like structure and a structure in which the two central basepairs ($\underline{A}^6$-$T^7$/$T^7$-$\underline{A}^6$) are Hoogsteen basepaired, while all others are Watson-Crick basepaired in a B-DNA like structure. However, this change does not seem to induce any large changes in the stability of the duplex as characterised by its melting temperature and thermodynamics. The main effect of the Hoogsteen basepairs on the overall structure is ~2-3Å narrowing of the minor groove and a corresponding widening of the major groove. To form a Hoogsteen basepair the 2'-deoxyadenosine moiety must change from *anti* to *syn* conformation: The replacement of the endocyclic 4'-oxygen in the natural pentose sugar with a methylene group makes the stereoelectronic anomeric and gauche effects in the resulting carbocyclic ring disappear, thereby making it more flexible. Additionally, the steric clash between the 4'-oxygen and the aglycone present in the O4'-*endo* conformation in the natural pentofuranose ring is not present in the carbocyclic counterpart, thereby making the *syn*/*anti* conformational transition more facile in the latter, promoting the Hoogsteen basepairing. It is interesting to note that only very few changes, mainly in α, δ and γ torsions, in the sugar-phosphate backbone seem to be necessary to accommodate the Hoogsteen basepairing.

It has recently been shown that a single 2'-deoxyaristeromycin ($\underline{A}$) substitution does not significantly alter the structure of an asymmetric DNA duplex (*34*). In our self-complementary and symmetric DNA duplex, this situation has however changed dramatically: The local structure at the center of a palindromic DNA sequence changes because the two $\underline{A}$ substitutions on the opposite strands are brought into close proximity of each other, thereby giving rise to an increased flexibility at the center which seems to be necessary for the bases to flip over from *anti* to *syn* and form the Hoogsteen basepairs. Further, the existence of the Hoogsteen basepaired conformer shows that this form is not just available through the flexibility of the duplex but it is the local structural changes (i.e. sequence and the site of modified A residue of our duplex which also allows it to be stabilised by *syn* $\underline{A}$/*anti T* basepairing. This is also supported by the fact that the bases of the two modified A residues always co-flip to give either two *syn* ot two *anti* $\underline{A}^6$– there is no detectable presence of any species where the base of the modified residue of one strand is in syn conformation and the one of the opposite strand is in anti. Further,

in an experiment where 2'-deoxyaristeromycin has been incorporated in both residue $\underline{A}^5$ and $\underline{A}^6$ in the same duplex (data not shown), as many as 4 major substructures can be observed in NMR under the same conditions as in this work.

This work shows that (i) there is very little energetic preference for the pentofuranose-based DNA world compared to the carbocyclic counterpart; (ii) the free-energies for forming the Watson-Crick and the Hoogsteen basepaired duplexes are very similar because there is very little energetic discrimination for the carbocyclic vis-á-vis pentofuranose world, and (iii) we expect the same to be true in the carbocyclic vis-á-vis pentofuranose based RNA world. Further, (iv) this work shows the limitations of 2'-deoxyaristeromycin-incorporation in DNA duplexes in order to increase nuclease stability as we can see how the structure of the DNA duplex starts to get disordered as the number of modified residues close to each other increases.

Further work is now in progress to show (i) what is the frequency of the Watson-Crick versus Hoogsteen basepair formation in a self-complementary carbocyclic-based 12mer DNA duplex; (ii) what is the preference for homo- or hetero-duplex formation when an equimolar amount of pentofuranose-based 12mer and carbocyclic-based 12mer are mixed together in a buffered aqueous solution, and finally, (iii) can a carbocyclic-based oligo DNA act as a template, or would a carbocylic nucleotide 5'-triphosphate be incorporated on a native DNA template, in a DNA polymerase based reaction.

***Acknowledgements***

Thanks are due to the Swedish Board for Technical Development (NUTEK), the Swedish Natural Science Research Council (NFR), the Swedish Research Council for Engineering Sciences (TFR), Stiftelsen f÷r Strategisk Forskning (SSF), Wallenbergsstiftelsen, the University of Uppsala and Forskningsrdn∑mnden (FRN) for generous financial support.

***References and Footnotes***

1.(a) Altmann, K-H., Kesselring, R. and Pieles U. (1996) Tetrahedron 52, 12699, (b) Portmann, S., Altmann, K-H., Reynes, N. and Egli, M. (1997) J. Am. Chem. Soc. 119, 2396

2.(a) Knorre, D. G., Vlassov, V. V., Zarytova, V. F., Lebedev, A. V. and Fedorova, O. S. (1994) in Design and Targeted Reactions of Oligonucleotide Derivates, CRC Press, Boca Raton, FL., (b) Puri, N. and Chattopadhyaya, J. (1999) Nucleosides & Nucleotides 18, 2785, (c) Damah, M. J., Wilds, C. J., Noronha, A., Brukner, I., Borkow, G., Arion,D. and Parniak, M. A. (1998) J. Am. Chem. Soc. 120, 12976

3.(a) Patel, D. J. (1992) Cur. Opin. Struct. Biol. 2, 345, (b) Brown, T. and Kennard, O. (1992) Cur. Opin. Struct. Biol. 2, 354, (c) Wang, A. H-J. (1992) Cur. Opin. Struct. Biol. 2, 361, (d) Cho, Y., Zhu, F. C., A., L. B. and Gorenstein, D. G. (1993) J. Biomol. Struct. Dynamics 11, 685 (e) Gorenstein, D. G. (1994) Chem. Rev. 94, 1315, (f) Mesmaeker, A. D.,Altmann, K-H., Waldner, A. and Wendeborn, S. (1995) Cur. Opin. Struct. Biol. 5, 343, (g) Krugh, T. R. (1994) Cur. Opin. Struct. Biol. 4, 351, (h) Schweitzer, B. I., Mikita, T., Kellogg, G. W., Gardner, K. H. and Beardsley, G. P. (1994) Biochemistry 33, 11460, (i) Gonzßlez, C., Stec, W., Reynolds, M. A. and James, T. L. (1995) Biochemistry 34, 4969,

4.Denisov, A. Y., Zamaratski, E. V., Maltseva, T. V., Sandstr÷m, A., Bekiroglu, S., Altmann, K-H., Egli, M. and Chattopadhyaya, J. (1998) J. Biomol. Struct. Dyn. 16, 547, and references therein for references to other NMR and X-ray work on Dickerson's dodecamer.

5. Marquez, V. E. and Lim, M-I. (1986) Med. Res. Rev. 6, 1

6. (a) Thibaudeau, C. and Chattopadhyaya, J. (1999) in Stereoelectronic Effects in Nucleosides and Nucleotides and their Structural Implications, Uppsala University Press, Sweden, (b) Bekiroglu, S., Thibaudeau, C., Kumar, A., Matsuda, A., Marquez, V. and Chattopadhyaya, J. (1998) J.Org. Chem 63, 5447, (c) Ossipov, D., Zamaratski, E., and Chattopadhyaya, J. (1999) Helv. Chim. Acta, 82, 2186

7. (a) Koole, L. H., Buck, H. M., Nyilas, A. and Chattopadhyaya, J. (1987) Can. J. Chem. 65,

2089, (b) Plavec, J., Tong, W. and Chattopadhyaya, J. (1993) J. Am. Chem. Soc. 115, 9734, (c) Plavec, J., Thibaudeau, C., Viswanadham, G., Sund, C. and Chattopadhyaya, J. (1994) J. Chem. Soc. Chem. Commun. 781, (d) Thibaudeau, C., Plavec, J., Garg, N., Papchikhin, A. and Chattopadhyaya, J. (1994) J. Am. Chem. Soc. 116, 4038, (e) Plavec, J., Thibaudeau, C. and Chattopadhyaya, J. (1994) J. Am. Chem. Soc. 116, 6558, (f) Plavec, J., Thibaudeau, C., Viswamadham, G.,Sund, C., Sandstr÷m, A. and Chattopadhyaya, J. (1995) Tetrahedron 51, 11775, (g) Thibaudeau, C., Plavec, J. and Chattopadhyaya, J. (1996) J. Org. Chem. 61, 266, (h) Plavec, J., Thibaudeau, C. and Chattopadhyaya, J. (1996) Pure Appl. Chem. 68, 2137, (i) Thibaudeau, C., F÷ldesi, A. and Chattopadhyaya, J. (1997) Tetrahedron 53, 14043, (j) Luyten, I., Thibaudeau, C. and Chattopadhyaya, J. (1997) J. Org. Chem. 62, 8800, (k) Luyten, I., Thibaudeau, C. and Chattopadhyaya, J. (1997) Tetrahedron 53, 6433, (l) Thibaudeau, C., Plavec, J. and Chattopadhyaya J. (1998) J. Org. Chem. 63, 4967

8. (a) Marquez, V. E., Ezzitouni, A., Russ, P., Siddiqui, M. A., Ford, H. J., Feldman, R. J., Mitsuya, H., George, C. and Barchi, J. J. J. (1998) J. Am. Chem. Soc. 120, 2780, (b) Altmann, K-H., Kesselring, R., Francotte, E. and Rihs, G. (1994) Tetrahedron Lett. 35, 2331, (c) Marquez, V. E., Siddiqui, M. A., Ezzitouni, A., Russ, P., Wang, J., Wagner, R. W. and Metteuci, M. D. (1996) J. Med. Chem. 39, 3739
9. J. Isaksson, T. Maltseva, P. Agback, X. Luo, A. Kumar, E. Zamratski and J. Chattopadhyaya, Nucleosides and Nucleotides, 18(6&7), 1593-1596 (1999). Earlier, we reported the preliminary solution structures of these interconverting WC/Hoogsteen duplexes for this molecule on the basis of an incomplete NMR constraint data set in a congress abstract. This is now thoroughly revised, and the full methodology and results are presented herein, including the thermodynamics and kinetics of the inter conversion. At a higher temperature (>50ºC), this interconverting WC/Hoogsteen duplex were earlier assumed to transform to a hairpinû type structure on the basis of insufficient evidence. Upon closer examina tion, this is found not to be true and is therefore rejected. In fact, the res onances that were attributed to the hairpin structure has its origin in the coalescence of the two sets of chemical shifts in the NMR-time scale due to the quick structural exchange of the interconverting WC/Hoogsteen duplex prior to melting (see Figures 10A-C).
10. (a) Saenger, W. (1988) in Principles of Nucleic Acid Structure, Springer-Verlag, New York, Berlin, Heidelberg, Tokyo, (b) Arnott, S. and Hukins, D. W. L. (1972) Biochem. Biophys. Res. Comm. 47, 1504
11. Sklenár, V. and Feigon, J. (1990) Nature 345, 836
12. (a) Maltseva, T. V., Altmann, K-H., Egli, M. and Chattopadhyaya, J. (1998) J. Biomol. Struct. Dyn. 16, 569, (b) Otting, G., Liepinsh, E., Farmer II, B. T. and Wthrich, K. (1991) J. Biomol. NMR 1, 209
13. Chary, K. V. R., Rastogi, V. K. and Govil, G. (1993) J. Magn. Reson. 102 B, 81
14. Brnger, A. T. (1990) X-PLOR 3.1, Manual. Yale University Press, New Haven, CT.
15. Varani, G., Aboul-ela, F. and Allain, F. H-T. (1996) Prog. NMR Spectrosc., 29, 51
16. Omichinski, J. G., Pedone, P. V., Felsenfeld, G., Gronenborn, A. M. and Clore, G. M. (1997) Nature Struct. Biol. 4, 122
17. Borgias, B. A., Thomas, P. D., Liu, H., Kumar, A. and James, T. L. (1993) Mardigras3.0/Corma5.0, Manual, University of California, San Francisco,CA.
18. Babcock, M. S., Pednault, E. P. D. and Olson, W. K. (1993) J. Biomol. Struct. Dyn. 11, 597
19. Van De Ven (1997) in Multidimensional NMR in Liquids, pp78-82, Wiley
20. Aurelia V2.1.3, Bruker Analytik GmbH
21. Overmars, F. (1997) in Conformational Aspects of Branched DNA, Dissertation, Ridderprint B.V., Ridderkerk
22. (a) Davis, T. M., McFail-Isom, L., Keane, E. and Williams, L. D. (1998) Biochemistry 37, 6975, (b) Ivanov, V. I., Minchenkova, L.E., Schyolkina,

A. K. and Poletayev, A. I. (1973) Biopolymers 12, 89, (c) Alen, F. S., Gray, D. M., Roberts, G. P. and Tonoko Jr., I. (1972) Biopolymers 11, 853, (d) Summers, M. F., Byrd, R. A., Gallo, K. A., Samson, C. J., Zon, G. and Egan, W. (1985) Nucl. Acids Res. 13, 6375

23. (a) Blommers, M. J. J., Van de Ven, F. J. M., Van der Marel, G. A., Van Boom, J. H. and Hilbers, C. W. (1991) Eur. J. Biochem. 201, 33, (b) Jaeger, J. A. and Tinoco Jr., I. (1993) Biochemistry 32, 12523
24. (a) Hosour, R. V., Govil, G. and Miles, H. T. (1988) Magn. Reson. Chem. 26, 927, (b) Gronenborn, A. M. and Clore, G. M. (1985) Prog. NMR Spectrosc. 17, 1-31, (c) Van de Ven, F. J. M. and Hilbers, C. W. (1998) Eur. J. Biochem. 178, 1
25. (a) Nerdal, W., Hare, D. R. and Reid, B. R. (1989) Biochemistry 28, 10008, (b) Yamakage, S-I, Maltseva, T. V., Nilson, F. P., F÷ldesi, A. and Chattopadhyaya, J. (1993) Nucl. Acids Research 21, 5005
26. Conte, M. R., Bauer, C. J. and Lane, A. N. (1996) J. Biomol. NMR 7, 190
27. Rinkel, L. J. and Altona, C. (1987) J. Biomol. Struct. Dyn. 4, 621
28. Chou, S-H., Zhu, L., Gao, Z., Cheng, J-W. and Reid, B. R. (1996) J. Mol. Biol. 264, 981
29. Kim, S-G., Lin, L-J. and Reid, B. R. (1992) Biochemistry 31, 3564
30. (a) Rongata, V. K., Jones, C. R. and Gorenstein, D. G. (1990) Biochemistry 29, 5245, (b) Chary, K. V. R., Rastogi, V. K. and Govil, G. (1993) J. Magn. Reson. 102 B, 81
31. Gorenstein, D. G. (1984) in Phosphorous-31 NMR: Principles and appli cations, Academic Press, New York
32. SYBYL 6.2 (1995), Tripos, Inc., St. Louis, Missouri
33. (a) Sasosekharan, V. (1972) Jerus. Symp. Quant. Chem. Biochem. 5, 247 260, (b) Lugovskoi, A. A. and Dashevskii, V. G. (1972) Mol. Biol. (USSR) 6, 354
34. Smirnov S., Johnson F., Marumoto R. and de los Santos C. (2000) J. Biomol. Struct. Dyn. 17, 981

*Date Received: December 22, 2000*

**Communicated by the Editor Ramaswamy H. Sarma**